# Mammalian microtubule P-body dynamics are mediated by nesprin-1

Dipen Rajgor,[1] Jason A. Mellad,[1] Daniel Soong,[1] Jerome B. Rattner,[2] Marvin J. Fritzler,[2] and Catherine M. Shanahan[1]

[1]Cardiovascular Division, BHF Centre of Excellence, James Black Centre, King's College London, London SE5 9NU, England, UK
[2]Department of Biochemistry and Molecular Biology, University of Calgary, Calgary T2N 4N1, Alberta, Canada

Nesprins are a multi-isomeric family of spectrin-repeat (SR) proteins, predominantly known as nuclear envelope scaffolds. However, isoforms that function beyond the nuclear envelope remain poorly examined. Here, we characterize p50$^{Nesp1}$, a 50-kD isoform that localizes to processing bodies (PBs), where it acts as a microtubule-associated protein capable of linking mRNP complexes to microtubules. Overexpression of dominant-negative p50$^{Nesp1}$ caused Rck/p54, but not GW182, displacement from microtubules, resulting in reduced PB movement and cross talk with stress granules (SGs). These cells disassembled canonical SGs induced by sodium arsenite, but not those induced by hydrogen peroxide, leading to cell death and revealing PB–microtubule attachment is required for hydrogen peroxide-induced SG anti-apoptotic functions. Furthermore, p50$^{Nesp1}$ was required for miRNA-mediated silencing and interacted with core miRISC silencers Ago2 and Rck/p54 in an RNA-dependent manner and with GW182 in a microtubule-dependent manner. These data identify p50$^{Nesp1}$ as a multi-functional PB component and microtubule scaffold necessary for RNA granule dynamics and provides evidence for PB and SG micro-heterogeneity.

## Introduction

Nesprins are a family of cellular scaffolds and linkers, composed of spectrin repeats (SRs) and a C-terminal nuclear envelope (NE) targeting KASH (Klarsicht/ANC-1/Syne homology) transmembrane domain (Zhang et al., 2001, 2005; Warren et al., 2005; Mellad et al., 2011; Rajgor and Shanahan, 2013). To date, four nesprin proteins have been identified, encoded by separate genes and capable of generating multiple tissue-specific isoforms. The full-length gene products of nesprin-1 and -2 contain a pair of N-terminal calponin homology domains that bind F-actin (Zhang et al., 2002). Nesprin-3 interacts with plectin, a cytoskeletal cross-linker that associates nesprin-3 with intermediate filaments (Wilhelmsen et al., 2005). Nesprin-4 interacts with Kif5B, a subunit of kinesin-1, and functions in nuclear migration and cell polarity (Roux et al., 2009; Horn et al., 2013). At the NE, nesprins form high-order structures called the linker of the nucleoskeleton and cytoskeleton (LINC) complex (Crisp et al., 2006; Stewart-Hutchinson et al., 2008; Mellad et al., 2011), which connects the nuclear lamina to the cytoskeleton.

In addition to nuclear–cytoskeletal coupling, scaffolding roles for nesprin-1 and -2 have been identified beyond the NE for KASH-less isoforms. The nesprin-1 isoform GSRP-56 localizes to the Golgi and regulates its structure (Kobayashi et al., 2006), whereas KASH-less nesprin-2 scaffolds ERK1/2 complexes in promyelocytic leukemia bodies and regulates vascular smooth muscle cell (VSMC) proliferation (Bernardi and Pandolfi, 2007; Warren et al., 2010). Other KASH-less isoforms include Drop-1 and CPG2, which are down-regulated in cancers and required for synaptic plasticity, respectively (Cottrell et al., 2004; Marmé et al., 2008).

Recently, we identified additional KASH-less tissue-specific nesprin-1 and -2 isoforms, suggesting new intracellular scaffolding functions for nesprins (Rajgor et al., 2012). In this report, we show that one of these, p50$^{Nesp1}$, localizes and interacts with a family of RNA-binding proteins in processing bodies (P-bodies/PBs). PBs are dynamic, nonmembranous domains containing nontranslating mRNAs and proteins involved in post-transcriptional

D. Rajgor and J.A. Mellad contributed equally to this paper.

Correspondence to Catherine M. Shanahan: cathy.shanahan@kcl.ac.uk

Abbreviations used in this paper: co-IP, co-immunoprecipitation; $H_2O_2$, hydrogen peroxide; HDF, human dermal fibroblast; KASH, Klarsicht/ANC-1/Syne homology; MAP, microtubule-associated protein; miRISC, miRNA-induced silencing complex; MT, microtubule; MTT, 3-[4,5-dimethylthiazol-2-yl]-2,5-diphenyltetrazolium bromide; NE, nuclear envelope; PB/P-body, processing body; SA, sodium arsenite; SG, stress granule; SR, spectrin repeat; VSMC, vascular smooth muscle cell.



The Rockefeller University Press $30.00
J. Cell Biol. Vol. 205 No. 4 457–475
www.jcb.org/cgi/doi/10.1083/jcb.201306076

processes, including mRNA decapping (e.g., Dcp1/2, Lsm1-7), mRNA degradation (e.g., XRN1), nonsense-mediated decay (e.g., hUPF1, hSMG5/7), translational repression (e.g., Rck/p54, eIF4E-T), and miRNA-mediated gene silencing (e.g., Argonautes, GW182, Rck/p54; Eulalio et al., 2007a; Moser and Fritzler, 2010). The presence of mRNA species in PBs, including mRNA decay intermediates and miRNAs, suggests they are likely to be functional entities (Sheth and Parker, 2003; Nathans et al., 2009; Castilla-Llorente et al., 2012). Additionally, mRNAs within PBs are capable of being released and translated onto polysomes (Brengues et al., 2005; Balagopal and Parker, 2009). Thus, PBs are likely to function as post-transcriptional regulatory hubs by acting as reservoirs for nontranslating mRNAs. Furthermore, PBs are anchored to microtubules (MTs) and are capable of moving within the cytosol (Aizer et al., 2008; Lindsay and McCaffrey, 2011).

During stress, related RNA stress granules (SGs) form (Anderson and Kedersha, 2008, 2009). SGs are composed of collapsed translation initiation complexes and RNA-binding proteins involved in several aspects of cellular metabolism. Their formation is thought to be essential for cell survival, as they accommodate transcripts for housekeeping proteins during stress to facilitate the preferential translation of proteins and repair enzymes required to deal with the insult (Arimoto et al., 2008). The frequent association observed between SGs and PBs is thought to mediate an exchange process where transcripts can be transferred to PBs for degradation or storage (Kedersha et al., 2005). Although PBs and SGs are structurally distinct, eIF4E, XRN1, and TTP are present in PBs in unstressed cells and capable of relocalizing to SGs under stress, suggesting bidirectional exchange occurs (Kedersha et al., 2005).

Mechanisms surrounding PB formation, disassembly, and dynamic properties related to SG association remain poorly characterized. In this study, we show $p50^{Nesp1}$ connects PBs to MTs by acting as a microtubule-associated protein (MAP). Moreover, the dynamic properties of PB–MT attachment via $p50^{Nesp1}$ are investigated with respect to PB motion and their ability to cross talk with SGs. Additionally, we demonstrate that $p50^{Nesp1}$ interacts with core miRNA-induced silencing complex (miRISC) components and is required for miRNA function and PB stability.

## Results

### Non-NE nesprin-1 variants

A polyclonal antibody, pAbN4, was generated against a peptide sequence in SR49 of nesprin-1, which is present in multiple KASH-less isoforms that display nucleolar and cytoplasmic localizations when ectopically expressed in cells (Fig. 1 A; Rajgor et al., 2012).

Immunofluorescence microscopy using pAbN4 on U2OS cells, human dermal fibroblasts (HDFs), and VSMCs detected nuclear structures that colocalized with the nucleolar marker fibrillarin and recognized one or more nucleoli per cell (Fig. 1 B and Fig. S1, A and B). pAbN4 also exhibited some diffuse cytoplasmic staining, but most obviously detected multiple cytoplasmic foci that varied in size and number (Fig. 1 B); U2OS cells had 5 or more foci, VSMCs rarely expressed more than 4, and HDFs had the greatest variation with some cells foci-less and others displaying up to 20 (Fig. 1 C).

NE localization was not observed in these cell lines, suggesting they do not express large nesprin-1 KASH domain variants. However, nuclear rims were detected in C2C12 myoblasts, showing pAbN4 is capable of detecting large KASH domain variants containing SR49. C2C12 cells had no nucleolar staining but had a large number of cytoplasmic foci (Fig. S1 C).

Although nucleolar and diffuse cytoplasmic stainings were expected based on exogenous $p31^{Nesp1}$, $p23^{Nesp1}$, and $p12^{Nesp1}$ localizing to the nucleolus in HDFs and cytosol in U2OS cells (Rajgor et al., 2012), cytoplasmic foci staining was not. Peptide blocking pAbN4 diminished all nucleolar and cytosolic staining, verifying pAbN4 specificity (Fig. 1 D). In addition, a second polyclonal, pAbN5, created to another peptide sequence in SR49 also labeled multiple cytoplasmic foci and the cytosol. Unlike pAbN4 it labeled the nuclear matrix and not the nucleolus, with all localizations lost by peptide blocking (Fig. 1 D). Taken together, these data suggested that these cytoplasmic foci contained a bona fide nesprin-1 isoform.

### Nesprin-1 localizes to mRNA processing bodies

Transmission immunoelectron microscopy was performed to identify the nature of the cytoplasmic foci. Gold labeling was apparent around the pericentriolar material and also localized to multiple electron-dense, nonmembranous foci surrounding the centrosome in HDFs (Fig. 2 A)—all features characteristic of P-bodies/PBs (Eystathioy et al., 2002).

pAbN4 cytoplasmic foci colocalized with the core RISC (RNA-induced silencing complex) regulator GW182, translational regulator RFP-Rck/p54, and de-capping cofactors Hedls and Dcp1a-YFP within PBs of U2OS cells (Fig. 2 B). Likewise, the cytoplasmic foci detected with pAbN5 also colocalized with Hedls (Fig. 2 C), and those detected in C2C12 cells colocalized with GW182 (Fig. S1 D).

Immunostaining for eIF3-η, which labels SGs in arsenite-stressed cells, often juxtaposed with the nesprin-1 foci, a typical phenomenon observed between PBs and SGs (Fig. 2 D) (Kedersha et al., 2005).

### $p50^{Nesp1}$ associates with Dcp1a, Rck/p54, and Ago2 complexes, but not GW182

To identify components associated with nesprin-1 in PBs, pAbN4 immune complexes from U2OS cells were probed for PB proteins. Dcp1a, Rck/p54, and Ago2 were detected with nesprin-1; however, GW182 was absent. Similarly, pAbN5 also precipitated Dcp1a and Ago2 (unpublished data). All interactions were abolished when lysates were predigested with RNase A, indicating nesprin-1 complexes are bridged by RNA species (Fig. 3 A). When reverse co-immunoprecipitations (co-IPs) were performed, Dcp1a, Rck/p54, and Ago2 precipitated a 50-kD nesprin-1 isoform corresponding to $p50^{Nesp1}$. GW182 immune complexes did not contain any nesprin-1 isoforms detected by pAbN4 (Fig. 3 B). Immune complexes could not be probed with pAbN5, as this antibody was unsuitable for immunoblotting (unpublished data).

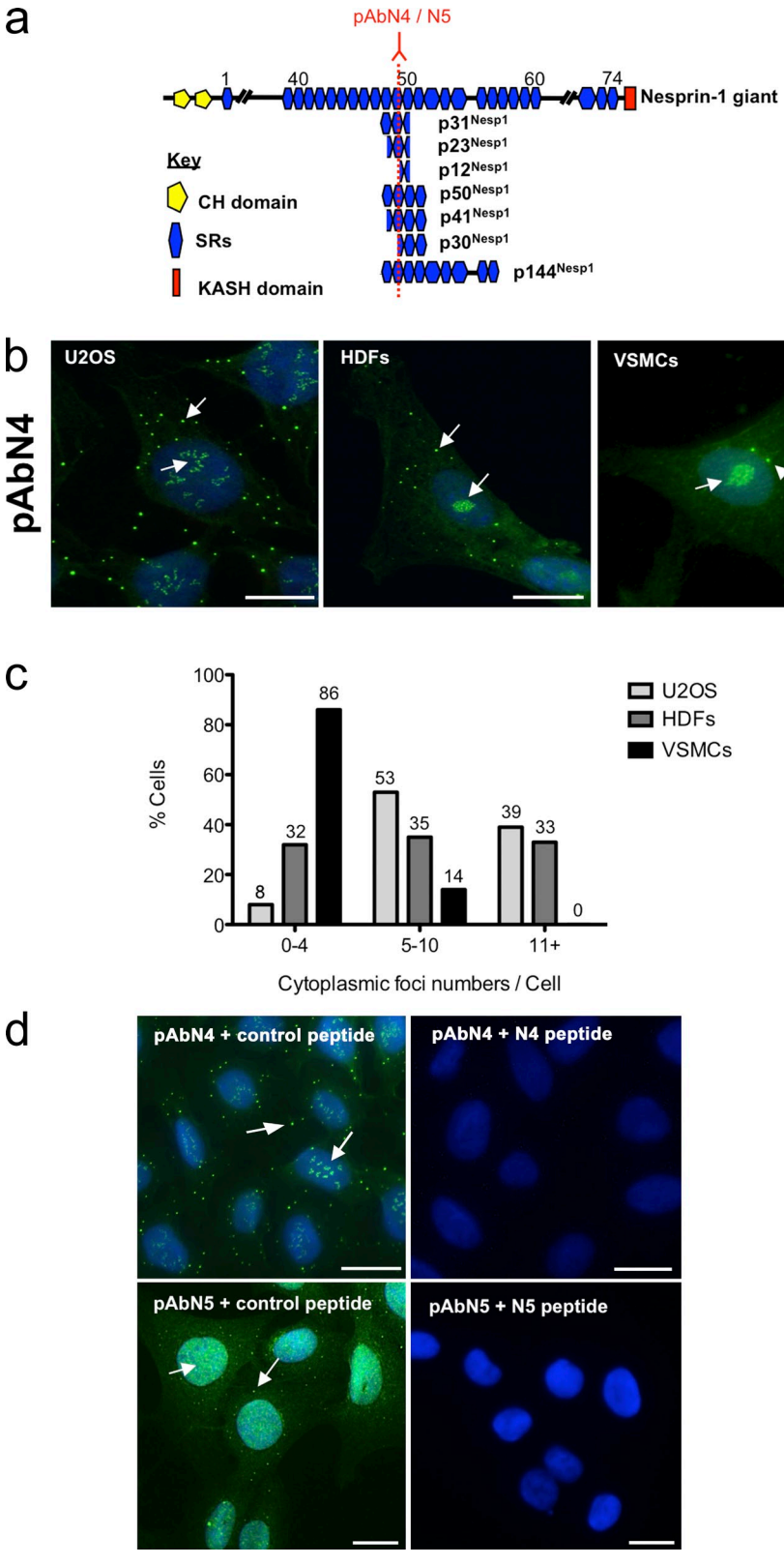


Figure 1. **Subcellular localization of nesprin-1 isoforms.** (a) Schematic of nesprin-1 isoforms containing the pAbN4 epitope present in SR49 of nesprin-1 giant. SRs of nesprin-1 giant are numbered in increments of 10, with some excluded for simplicity. (b) In U2OS cells, HDFs, and VSMCs, pAbN4 labels nuclear structures and cytoplasmic foci as shown by arrows. (c) Graph showing percentage of cells showing 0–4, 5–10, or more than 11 foci ($n$ = 300). (d) pAbN4 and N5 stainings shown by arrows in control peptide images were diminished by peptide blocking. Bars, 10 μM.

p50$^{Nesp1}$ GST fusion constructs were created to map binding sites for its associated PB proteins. Full-length p50$^{Nesp1}$, its first two SRs (p50NT), last two SRs (p50CT) and the four individual SRs (p50SR1, p50SR2, p50SR3, and p50SR4) were GST tagged and incubated with lysates from U2OS. Rck/p54, Dcp1a, and Ago2 pulled down with full-length GST-p50$^{Nesp1}$ and GST-p50NT. More specifically, GST-p50SR1 pulled down Rck/p54 and Ago2 but not Dcp1a, which associated with GST-p50SR2 instead. Consistent with our co-IPs, GW182 did not interact with any GST constructs (Fig. 3 C).

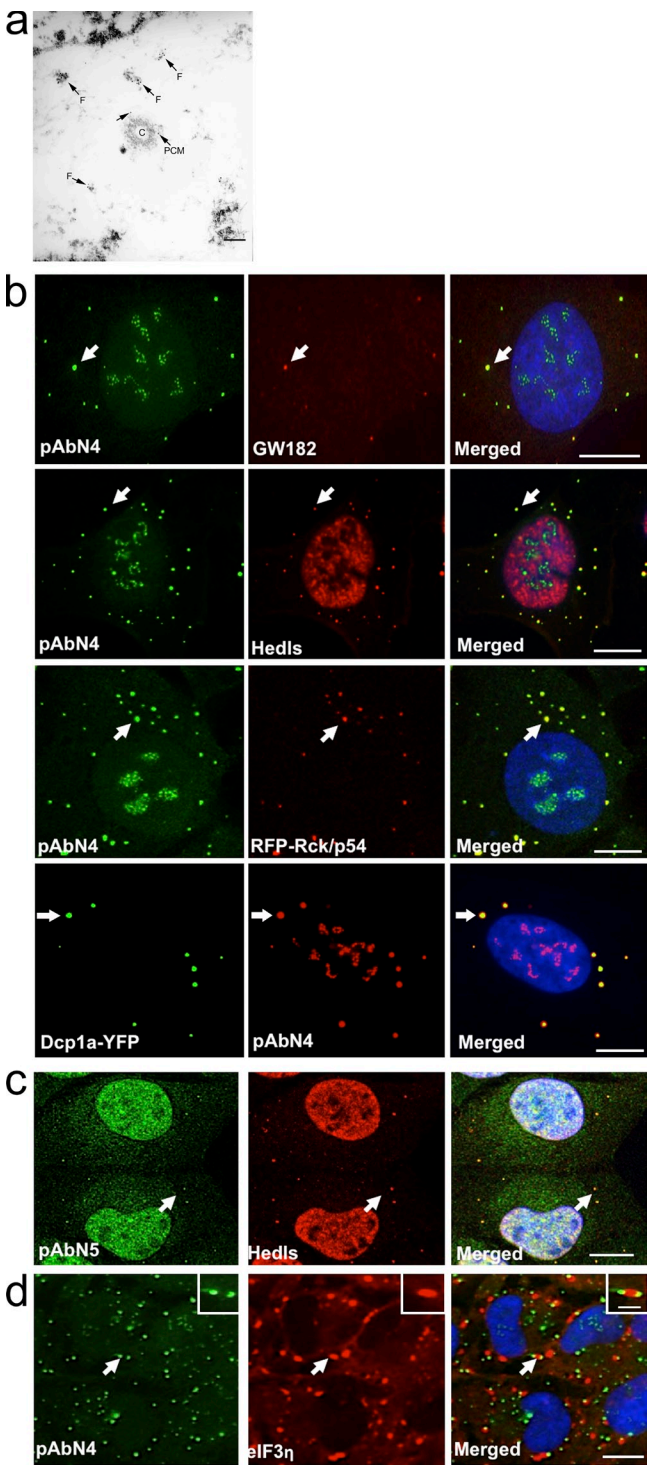


Figure 2. **Nesprin-1 foci are PBs.** (a) Transmission immunoelectron microscopy localized nesprin-1 to electron-dense, nonmembrane-bound foci (F) flanking the centrosome (C) and the pericentriolar material (PCM) in HDFs. Arrows point to either F or PCM. Bar, 250 nm. (b) pAbN4 cytoplasmic foci colocalized with endogenous GW182 and Hedls and ectopic RFP-Rck/p54 and Dcp1a-YFP in U2OS cells as shown by arrows. (c) pAbN5 cytoplasmic foci colocalized with Hedls as shown by arrows. (d) pAbN4 foci juxtaposed to sodium arsenite induced eIF3η stress granules. Arrows point to region shown in inset. Bars: (main panels) 10 µm; (d, insets) 2 µm.

In addition, immune complexes from Flag-p50$^{Nesp1}$–transfected U2OS cells also contained Ago2, Dcp1a, and Rck/p54, but not GW182. Flag-p50NT was also capable of weakly co-precipitating Ago2, Dcp1a, and Rck/p54 (Fig. 3 D). However, a truncated isoform, p31$^{Nesp1}$, which contains the SRs present in p50NT, was unable to co-immunoprecipitate any of these proteins, suggesting these interactions were specific to p50$^{Nesp1}$.

## p50$^{Nesp1}$ localizes to PBs and microtubules

To examine the effects of ectopic p50$^{Nesp1}$ on PBs, Flag-p50$^{Nesp1}$ was expressed in multiple cell lines. In VSMCs, which express a small number of PBs (Fig. 1 C), Flag-p50$^{Nesp1}$ localized to and induced PB formation. However, in U2OS cells and HDFs, but not VSMCs, Flag-p50$^{Nesp1}$ formed bundled structures reminiscent of cytoskeletal filaments. These structures did not contain F-actin or intermediate filaments, as no colocalization with phalloidin or vimentin was apparent (Fig. S2). However, the bundles strongly colocalized with α-tubulin, suggesting p50$^{Nesp1}$ may be a microtubule-associated protein (MAP) capable of direct interactions (Fig. 4 A). To examine this possibility, we performed in vitro MT cosedimentation assays. Full-length p50$^{Nesp1}$ and p50CT co-pelleted with polymerized MTs after ultra-centrifugation, but were not detected in pellets when MTs were absent. The SRs in p50NT remained in the supernatant after ultracentrifugation in the presence and absence of MTs, ruling out MT interaction with these SRs. Interestingly, SR3 and SR4 failed to pellet with MTs independently, indicating the MT binding of p50$^{Nesp1}$ requires both the C-terminal SRs in tandem. (Fig. 4 B).

In both U2OS cells and VSMCs, Flag-p50CT localized to MTs in a similar fashion to full-length p50$^{Nesp1}$ in U2OS cells, confirming MT association (Fig. 4 C). However, Flag-SR1, -SR2, -SR3, -SR4, and -p50NT all displayed diffusive cytoplasmic localizations in U2OS cells (Fig. 4 D).

## p50$^{Nesp1}$ recruits PBs to MTs

By interacting with PB proteins through its N-terminal SRs and MTs via its C-terminal SRs, we hypothesized p50$^{Nesp1}$ as a PB–MT linker. To explore this possibility, we examined Rck/p54 and GW182 PBs in U2OS cells transfected with Flag-p50$^{Nesp1}$. Rather than forming cytoplasmic foci, both proteins were recruited to and colocalized with p50$^{Nesp1}$ MTs. However, when Rck/p54 was assessed in U2OS cells expressing Flag-p50CT, it no longer coated MTs and instead localized adjacent to the MTs as detached foci. On the contrary, GW182 coated and colocalized with the MTs in Flag-p50CT–expressing cells (Fig. 5, A and B). Similar observations were seen with Rck/p54 and GW182 localizations in Flag-p50CT–transfected VSMCs (not depicted).

To demonstrate Rck/p54 recruitment and displacement from MTs was not an artifact of MT bundling, we examined Rck/p54 in U2OS cells transfected with prostate-derived sterile 20-like kinase 1α (PSK1α), a kinase which promotes similar MT bundling (Mitsopoulos et al., 2003). In these cells, Rck/p54 PBs colocalized strongly with PSK1α-induced MTs, confirming that displacement of Rck/p54 PBs from bundled MTs was a p50CT-specific event (Fig. S3).

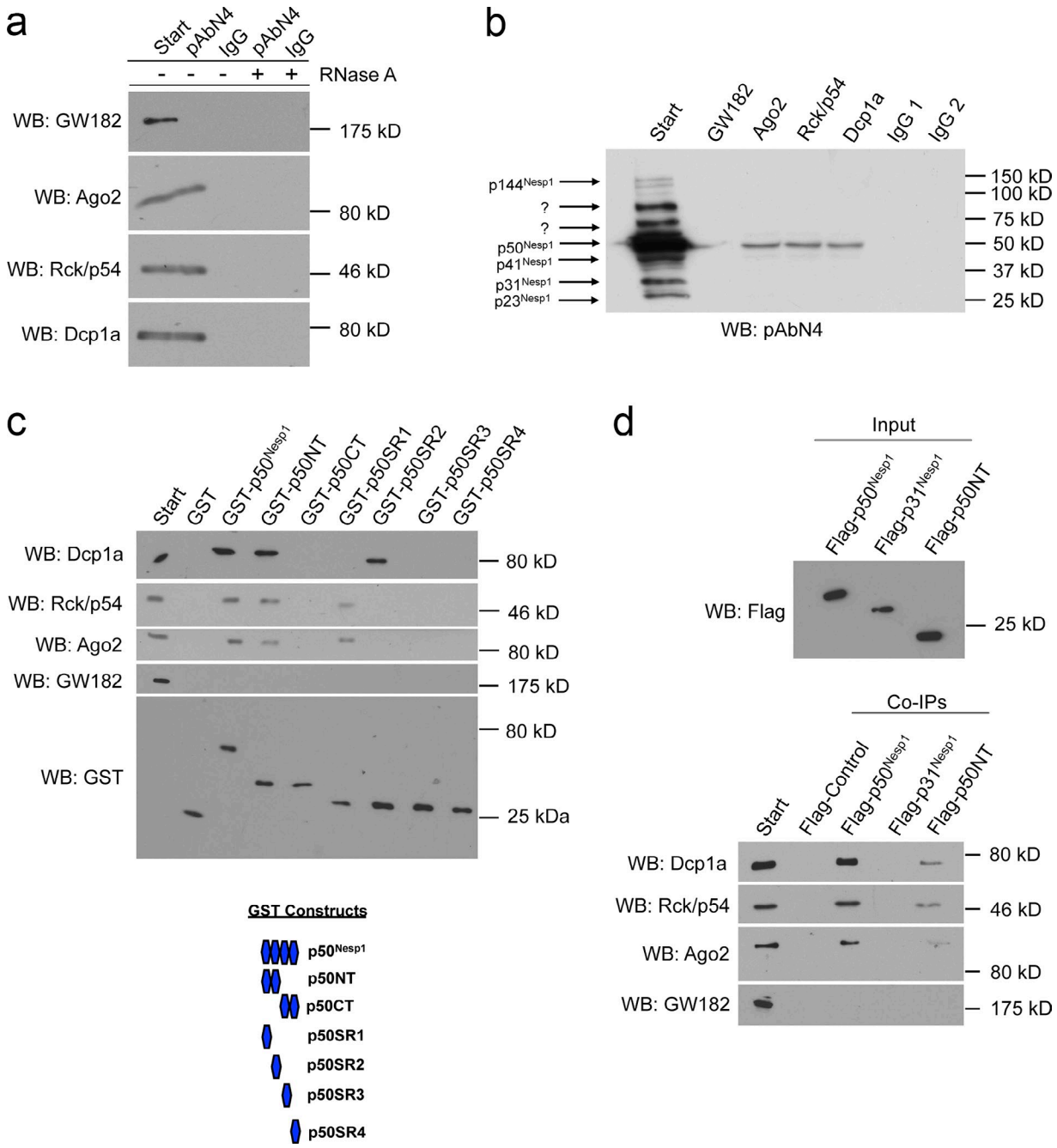


Figure 3. **p50$^{Nesp1}$ complexes with PB components.** (a) Dcp1a, Rck/p54, and Ago2 co-immunoprecipitate in an RNA-dependent manner with pAbN4 from U2OS cells. (b) p50$^{Nesp1}$ co-immunoprecipitates with Dcp1a, Rck/p54, and Ago2 in reverse co-IPs. (c) Dcp1a, Rck/p54, and Ago2 pull down with recombinant GST-p50$^{Nesp1}$ and GST-p50NT. Dcp1a specifically pulls down with p50SR2. Rck/p54 and Ago2 pull down with p50SR1. (d) Dcp1a, Rck/p54, and Ago2 co-immunoprecipitate with Flag-50$^{Nesp1}$ and Flag-p50NT, but not Flag-p31$^{Nesp1}$ in transfected U2OS cells.

Rck/p54 expression appeared to be enhanced in Flag-p50$^{Nesp1}$ cells compared with neighboring untransfected cells and Flag-p50CT cells, whereas GW182 expression appeared to be enhanced in both. Immunoblotting confirmed Rck/p54, Dcp1a, and Ago2 were more abundant in Flag-p50$^{Nesp1}$ cells compared with Flag-p50CT and Flag-control (empty flag vector), whereas GW182 expression was higher in both Flag-p50CT and Flag-p50$^{Nesp1}$ compared with Flag-control. α-Tubulin levels were elevated in both Flag-p50CT– and Flag-p50$^{Nesp1}$–transfected cells, indicative of MT stabilization (Fig. 5 C).

## p50$^{Nesp1}$–GW182 interaction is MT dependent

GW182 recruitment to Flag-p50$^{Nesp1}$ and Flag-p50CT bundles suggested that GW182–p50$^{Nesp1}$ association maybe MT dependent. Our binding studies were performed at 4°C and therefore MTs were likely to be depolymerized. Therefore, we re-performed co-IPs and GST pull-downs in U2OS cells pretreated with paclitaxel (taxol) for 24 h and co-IP buffer supplemented with taxol. Under these conditions, GW182 purified with pAbN4 immune complexes and also pulled down with GST-p50$^{Nesp1}$

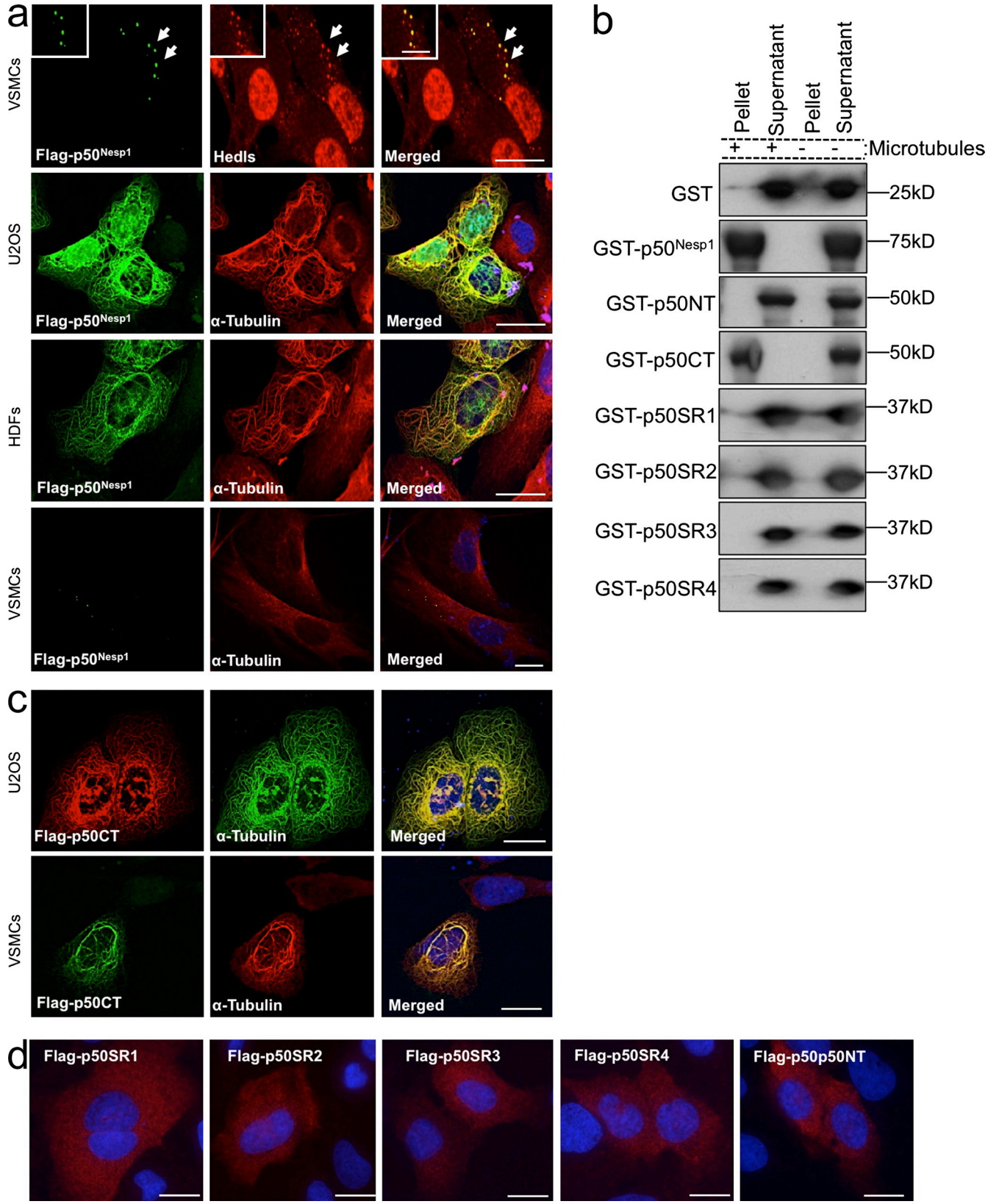


Figure 4. **p50$^{Nesp1}$ localizes to PBs and to MTs.** (a) Flag-p50$^{Nesp1}$ localized to and induced PB formation in VSMCs. Arrows point to colocalized foci shown in inset. In U2OS cells and HDFs, Flag-p50$^{Nesp1}$ localized to and bundled MTs. (b) GST-p50$^{Nesp1}$ and GST-p50CT co-pellet with MTs in vitro. In the absence of MTs, all constructs remained in the supernatant. (c) Flag-p50CT localizes to MTs in U2OS cells and VSMCs. (d) Flag-SR1, -SR2, -SR3, -SR4, and -p50NT were cytoplasmic in U2OS cells. Bars: (main panels) 10 µm; (a, insets) 2 µm.

and the MT-binding SRs in GST-p50CT (Fig. 5, D and E). When pAbN4 immune complexes were isolated in a similar manner in the presence of nocodazole from U2OS cells, GW182–nesprin interactions were abolished (Fig. 5 D), but not nesprin-1–Rck/p54, –Dcp1a, or –Ago2 interactions, suggesting $p50^{Nesp1}$ and GW182 interact in an MT-dependent manner.

### $p50^{Nesp1}$-MT scaffolds mediate PB motion

As Flag-p50CT was able to displace Rck/p54 from MTs in U2OS cells, PB motion was examined. Real-time tracking of Dcp1a-YFP in U2OS cells cotransfected either with Flag-$p50^{Nesp1}$, Flag-p50CT, or Flag-control was performed. Dcp1a-YFP PBs were traced for 2 min using time-lapse microscopy. The area covered by each PB was determined and used as a measure to determine motion. As described previously, PBs mainly localize in spatially confined regions with restricted motion (Aizer et al., 2008). Flag-control ($n = 84$) and Flag-$p50^{Nesp1}$ ($n = 262$) expressing cells covered areas of 0.0798 $\mu m^2$ and 0.0799 $\mu m^2$, respectively. However, cells expressing Flag-p50CT ($n = 116$) covered significantly reduced areas averaging 0.0514 $\mu m^2$, comparable coverage to Flag-control cells treated with nocodazole ($n = 429$) at 0.0501 $\mu m^2$ (Fig. 5 F).

To confirm that U2OS cells coexpressing Dcp1a-YFP and the respective Flag-protein were being recorded, culture dishes were stained for anti-Flag after filming. Every cell expressing Dcp1a-YFP also expressed Flag-$p50^{Nesp1}$ or Flag-p50CT, allowing easy selection for cotransfected cells. Interestingly, Flag-$p50^{Nesp1}$ no longer localized to MTs when cotransfected with Dcp1a-YFP and instead colocalized with it in PBs. However, Flag-p50CT localized to MTs with Dcp1a-YFP remaining unattached (Fig. 5 G). These data suggest that expression levels of proteins capable of binding to SR1+2 of $p50^{Nesp1}$ may determine whether ectopic $p50^{Nesp1}$ localizes to PBs or MTs. In support of this notion, immunoblotting confirmed VSMCs have increased levels of endogenous Dcp1a, Rck/p54, and Ago2 compared with U2OS cells, but similar levels of endogenous $p50^{Nesp1}$ and GW182. Furthermore, Flag-$p50^{Nesp1}$ promoted MT bundling when transfected into VSMCs depleted of Dcp1a using RNAi (Fig. S4).

### p50CT-expressing cells have reduced PB–SG connections and fail to disassemble $H_2O_2$-induced SGs

PBs and SGs associate in an MT-dependent manner during stress (Kedersha et al., 2005; Aizer et al., 2008); therefore, we next examined the dynamics of PB–SG associations by analyzing the distribution of β-globin reporter mRNA. Flag vectors were cotransfected into U2OS cells with a construct encoding β-globin mRNA with an MS2-binding site in its 3′UTR (pEF-7B-MS2bs) and a plasmid encoding a MS2-GFP coat protein, which tethers to the MS2-binding site and allows detection of β-globin transcripts (Kedersha et al., 2005). SGs were induced in transfected cells by 2 µM hydrogen peroxide ($H_2O_2$) for 1 h and stained for Rck/p54 PBs and PABP-1 SGs.

In cotransfected cells, the GFP-tethered β-globin transcripts localized to SGs and PBs. In Flag-control cells, ∼75% of cells showed one or more PB–SG association, with ∼80% of β-globin reporter detected in PBs. Conversely, in Flag-p50CT cells, only ∼10% of cells displayed at least one PB–SG association, with ∼80% of the reporter localizing to SGs, suggesting failure of mRNA species stored in SGs to transfer into PB compartments due to uncoupling of PBs from MTs (Fig. 6, A–C).

When U2OS cells were allowed to recover in normal media for 3 h, SGs in Flag-control cells disassembled and the tethered mRNA localized with PBs. However, SGs in Flag-p50CT cells failed to dissolve and accumulated β-globin transcripts (Fig. 6, A and C).

To determine if the hampered PB–SG dynamics in Flag-p50CT cells was specific for $H_2O_2$-induced stress, we re-performed these experiments in cells stressed with 0.5 mM sodium arsenite (SA) for 1 h. The number of PB–SG connections as well as β-globin localization was similar to that seen by cells treated with $H_2O_2$ (Fig. 6, D–F). However, SGs disassembled in both Flag-control and Flag-p50CT transfected cells when allowed to recover in normal media (Fig. 6 D). In agreement with a previous report, these experiments suggest $H_2O_2$-induced SGs differ from those induced by SA, and suggest there may be heterogeneity in the dynamic properties of SGs induced by different stressors (Emara et al., 2012).

To examine the dynamics of mRNA sorting and SGs in cells where the binding proteins associated with SR1+2 of $p50^{Nesp1}$ remained attached to MTs, we performed these experiments in cells transfected with Flag-$p50^{Nesp1}$. SGs induced by $H_2O_2$ or SA frequently associated with, or were in close proximity to, the bundled MTs detected by Rck/p54 staining (Fig. 6 G). These cells contained small amounts of the reporter mRNA in SGs, with the majority colocalizing with Rck/p54 on MTs, consistent with the localization of the reporter with Rck/p54 PBs in Flag-control cells. The presence of β-globin scattered along the MTs made quantification difficult. Therefore, to measure the efficiency of mRNA sorting within these cells, we quantified the number of SGs containing the β-globin reporter relative to empty ones in $H_2O_2$- and SA-treated cells. In Flag-control cells, ∼20% of SGs contained the reporter, whereas in Flag-$p50^{Nesp1}$ significantly more (∼30%) contained the reporter. However, β-globin mRNA was detected in ∼90% of SGs in Flag-p50CT cells, a significant increase compared with both Flag-control and Flag-$p50^{Nesp1}$ (Fig. 6, H and I). These findings indicate that there are changes in mRNA distribution in cells overexpressing $p50^{Nesp1}$ and p50CT; however, in Flag-$p50^{Nesp1}$ cells mRNA can be retained in complexes containing Rck/p54 and $p50^{Nesp1}$ binding partners, whereas in Flag-p50CT cells, where PBs are displaced from MTs, mRNA cannot be distributed into Rck/p54 PBs. Like Flag-control cells, $H_2O_2$- and SA-induced SGs disassembled during recovery in Flag-$p50^{Nesp1}$ cells, indicating that retention of PBs onto MTs has no effect on SG disassembly. (Fig. 6 G).

### $H_2O_2$ triggers cell death in Flag-p50CT–expressing cells

We performed 3-[4,5-dimethylthiazol-2-yl]-2,5-diphenyltetrazolium bromide (MTT) assays to determine whether the SG disassembly defects induced by Flag-p50CT in $H_2O_2$-treated cells caused toxicity. After applying $H_2O_2$ or SA onto cells for 1 h, MTT readings were performed hourly for up to 8 h in recovering cells. Mild cellular toxicity was observed 4–5 h into

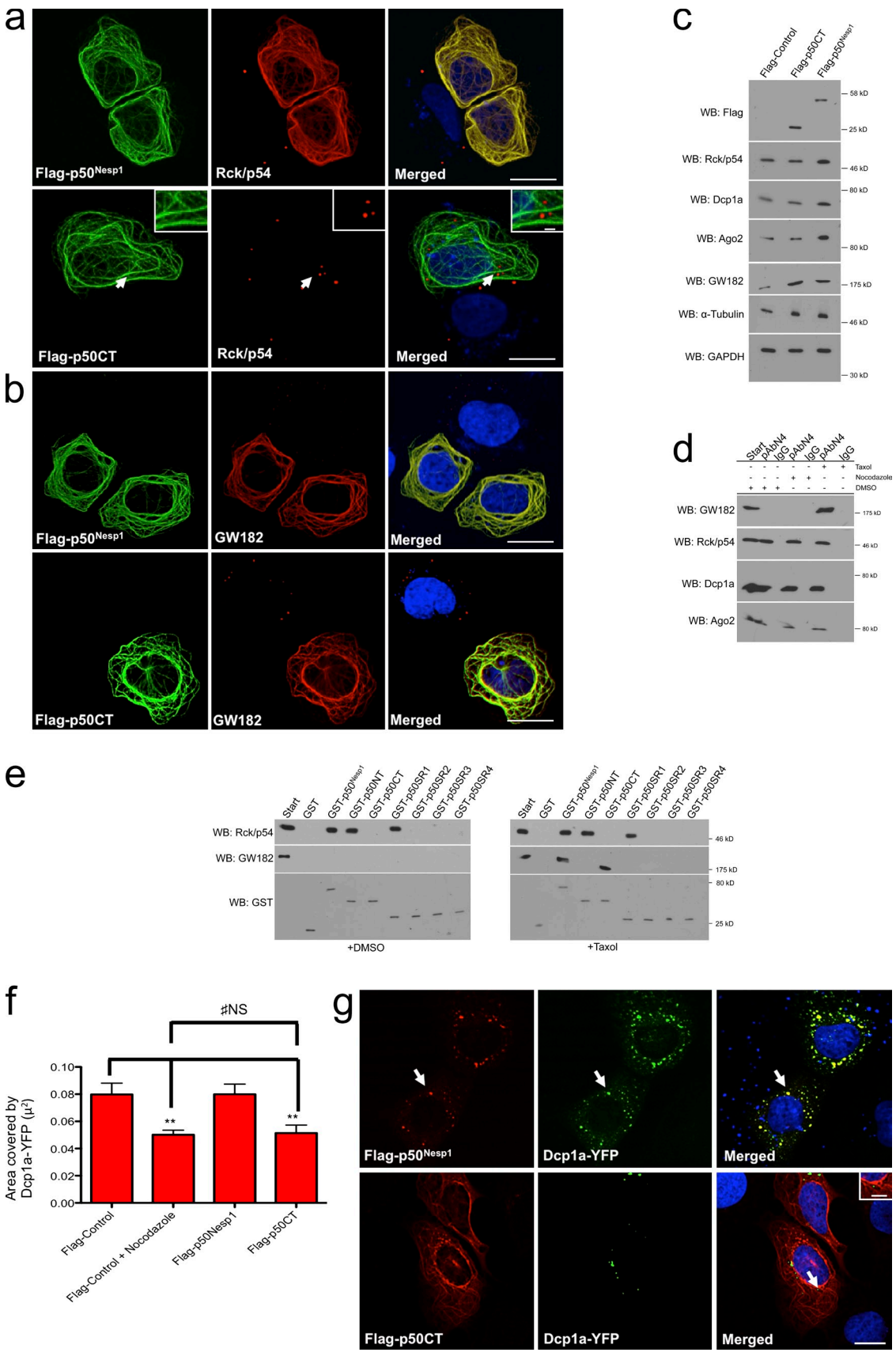


Figure 5. **p50$^{Nesp1}$ links PBs to microtubules (MTs) and regulates PB motion.** (a) Flag-p50$^{Nesp1}$ recruits Rck/p54 to MTs in U2OS cells. Flag-p50CT displaces Rck/p54 PBs from MTs. Arrows point to region shown in inset. (b) Flag-p50$^{Nesp1}$ and Flag-p50CT recruit GW182 to MTs. (c) Western blot showing levels of PB components and tubulin in U2OS cells transfected with Flag-p50$^{Nesp1}$, -p50CT, and -control (empty flag vector). GAPDH served as a loading control.

recovery in Flag-p50CT cells treated with $H_2O_2$ and more severe toxicity was observed after 7 h, and this was confirmed by time-lapse video microscopy that showed cell death. By contrast, no toxicity or death was seen in Flag-p50CT cells stressed with SA. Similarly, Flag-control or Flag-p50$^{Nesp1}$–transfected cells did not display any toxic symptoms after $H_2O_2$ or SA treatment (Fig. 7, A and B).

### p50$^{Nesp1}$ knock-down eliminates PBs

A panel of siRNAs was designed to examine PBs in p50$^{Nesp1}$-depleted cells. si-83 and si-90 were created to target the first and last coding exons of p50$^{Nesp1}$, respectively. si-136 was created toward the C terminus of the nesprin-1 giant to target KASH isoforms and serve as a negative control (Fig. 8 A). To validate the efficiency of these siRNAs, we measured nesprin-1 knockdown using pAbN4 and a previously described monoclonal antibody generated to SRs near the KASH domain of nesprin-1, to detect NE isoforms (Randles et al., 2010).

si-83 and si-90 knocked down p50$^{Nesp1}$, p31$^{Nesp1}$, 144$^{Nesp1}$, and an unknown ∼75-kD variant detected by pAbN4. Additionally, si-90 eliminated p41$^{Nesp1}$, whereas the nontargeting si-83 had no effect on its expression. si-136 had no effect on the expression levels of any nesprin-1 isoform detected by immunoblotting with pAbN4 (Fig. 8 B). si-136 reduced NE staining in U2OS cells detected by the C-terminal monoclonal, indicating it is capable of knocking down KASH-containing isoforms. However, si-83 did not reduce NE staining. Taken together, these data suggest that U2OS cells do not express large nesprin-1 KASH isoforms containing SR49, supporting the absence of NE staining in U2OS cells by pAbN4 (Fig. S5).

We used pAbN4, GW182, and Rck/p54 staining to assess PBs in nesprin-1–depleted U2OS cells (Fig. 8, C and D). RNAi with si-136 showed no difference in PB phenotype to controls, indicating KASH isoforms have no involvement in PB structures. In contrast, si-83 and si-90 both eliminated nesprin-1, GW182, and Rck/p54 foci in up to 80% of cells (Fig. 8 E). Nucleolar knockdown was not observed by any of the siRNAs, suggesting nucleolar staining by pAbN4 may be artifactual.

To identify which SRs were central for PB structure, we created si-83–resistant Flag-p50$^{Nesp1}$ and Flag-p50NT constructs to perform rescue experiments. Flag-p50$^{Nesp1}$ recruited Rck/p54 and GW182 to MTs in U2OS cells transfected with si-83. Interestingly, Flag-p50NT rescue reformed Rck/p54 and GW182 PBs, even though the construct localized diffusively within the cytosol rather than directly to PBs (Fig. 8 F). Flag-p50$^{Nesp1}$ or Flag-p50NT plasmids containing the correct si-83 seed region were not detected in si-83–transfected cells (unpublished data). In Flag-p50CT rescue cells, GW182 was recruited to MTs; however, Rck/p54 PBs were not detected (Fig. 8 F).

### p50NT SRs mediate miRISC function

The loss of macroscopic PBs does not necessarily imply loss of function of mRNA-processing pathways (Chu and Rana, 2006; Eulalio et al., 2007b). p50$^{Nesp1}$ binding partners Rck/p54, GW182, and Ago2 are core components of the miRISC. Therefore, we used the Let-7a miRISC luciferase reporter assay to assess if p50$^{Nesp1}$ is required for miRNA function (Chu and Rana, 2006; Lytle et al., 2007; Johnston et al., 2010). The psi-CHECK2-let-7X3 vector encoding luciferase contains 3× Let-7 miRNA-binding sites within its 3′UTR, and when transfected into cells expressing endogenous Let-7, luciferase expression is translationally repressed. However, knockdown of proteins involved in the miRISC pathway reduces silencing of the reporter and enhances luciferase expression. Knockdown of p50$^{Nesp1}$ using si-83 or si-90, but not si-136, significantly reduced miRISC activity in U2OS cells. Rck/p54 knockdown served as a positive control (Fig. 9 A). Similar effects on miRISC activity and PB number were also observed when these experiments were performed in VSMCs (unpublished data).

Flag-p50$^{Nesp1}$ was able to rescue miRISC function in si-83–transfected cells, confirming miRISC attenuation was due to p50$^{Nesp1}$ knockdown and not depletion of other nesprin-1 isoforms. Furthermore, a similar rescue was achieved by Flag-p50NT, but not by the MT binding Flag-p50CT or the individual four SRs, implying SR1+2 together make up the scaffold for translationally repressed mRNPs (Fig. 9, B and C). However, p31$^{Nesp1}$, which also contains the p50NT SRs, was unable to rescue miRISC activity (unpublished data).

Finally, to determine whether p50$^{Nesp1}$ had silencing capabilities independent of miRNAs, like GW182, we tethered V5-λN-p50$^{Nesp1}$ to a *Renilla* luciferase reporter with 5boxB elements in its 3′UTR. However, no significant changes in luciferase activity were observed (Fig. 9 D). Therefore, it appears p50$^{Nesp1}$ cannot directly induce translational repression and may require association with GW182, Ago2, Rck/p54, and other proteins along with miRNAs to facilitate silencing.

## Discussion

Here, we characterized a novel KASH-less nesprin-1 isoform, p50$^{Nesp1}$, which localizes to PBs and links them to MTs. p50$^{Nesp1}$ is important for PB dynamic motion and ability to associate and cross talk with SGs, and is the first SR-containing protein found to localize to PBs and act as a core miRISC component.

### p50$^{Nesp1}$ localizes and interacts with PB proteins and MTs

The cytoplasmic foci detected by pAbN4 and N5 colocalized with PB but not SG proteins. We identified p50$^{Nesp1}$ enriched in mRNPs with Rck/p54, Ago2, and Dcp1a, and mapped the binding

(d) pAbN4 co-IPs from U2OS cells in the presence of DMSO, nocodazole, and taxol were probed for PB proteins. (e) GST pull-downs performed in U2OS cells treated with DMSO or taxol. (f) Dcp1a-YFP PBs were tracked by time-lapse microscopy for 2 min to determine area covered by PBs in cells expressing Flag-control ($n$ = 83), Flag-p50$^{Nesp1}$ ($n$ = 262) and Flag-p50CT ($n$ = 116). Flag-control cells treated with 10 µg/ml nocodazole served as a positive control ($n$ = 429). #NS, not significant; **, P < 0.01; one-way ANOVA, Bonferroni post-hoc test. (g) Cells expressing Flag-p50$^{Nesp1}$ or Flag-p50CT also express Dcp1a-YFP. Arrows in top panel point to colocalized foci. Arrows in bottom panel point to region shown in inset. Bars: (main panels) 10 µm; (a and g, insets) 2 µm.

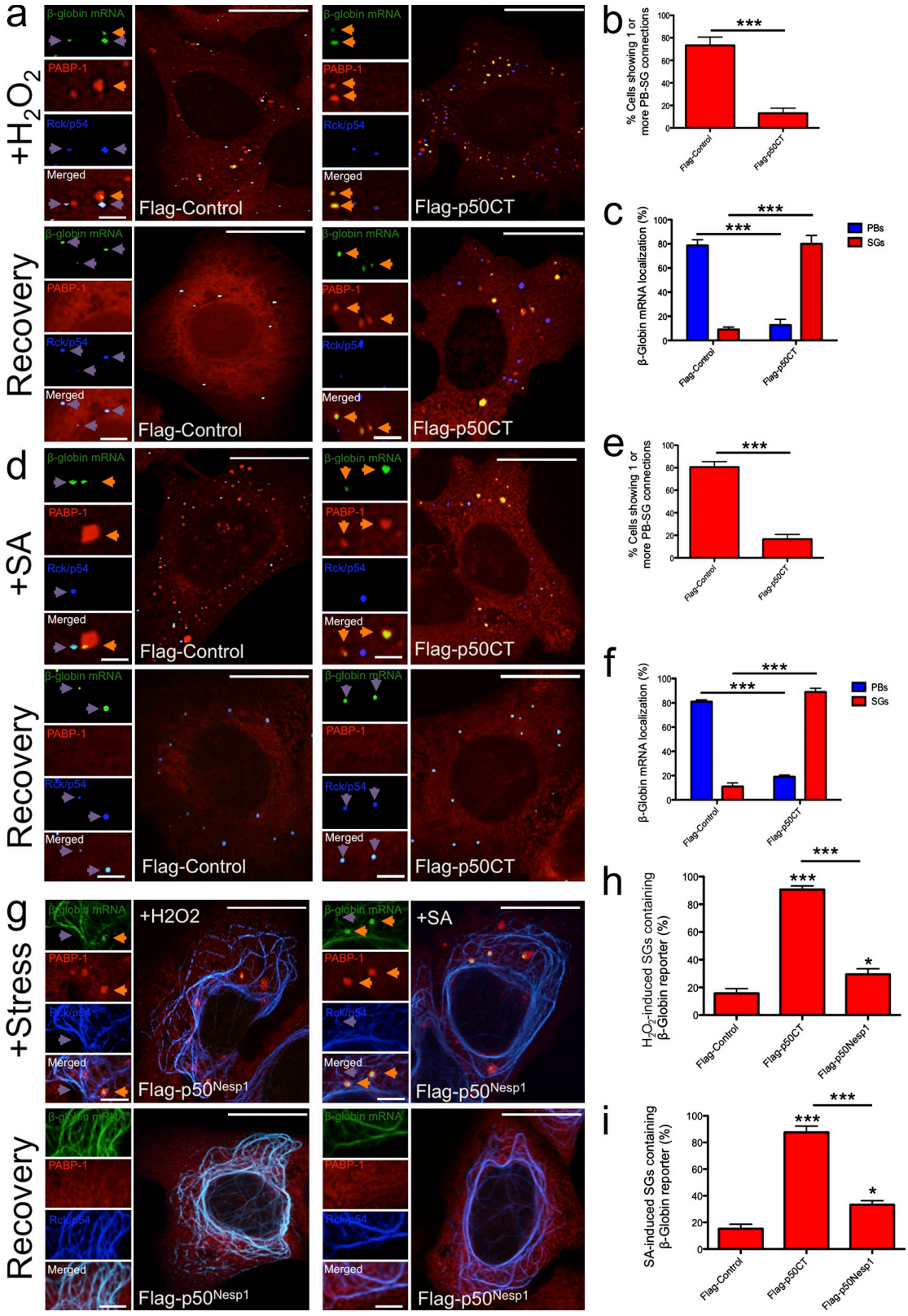


Figure 6. **p50$^{Nesp1}$ is required for PB–SG association.** (a) Rck/p54 PBs (blue) and PABP-1 SGs (red) in Flag-control and Flag-p50CT–transfected U2OS cells treated with $H_2O_2$ and allowed to recover. Orange arrows point to β-globin mRNA (green) in SGs and purple arrows in PBs. (b) Flag-p50CT cells ($n$ = 300) had significantly fewer cells showing one or more PB–SG connection relative to Flag-control cells ($n$ = 300). (c) Flag-control cells ($n$ = 300) accumulated significantly more β-globin mRNA in PBs, whereas Flag-p50CT cells ($n$ = 300) had significantly more reporter in SGs. (d–f) As in a–c, respectively, but with SA. ***, P < 0.001, Student's $t$ test. (g) Rck/p54, PABP-1, and β-globin in Flag-p50$^{Nesp1}$ cells treated with $H_2O_2$ or SA and allowed to recover. Orange arrows point to β-globin in SGs and purple arrows to microtubules. (h) Percentage of $H_2O_2$-induced SGs containing β-globin reporter. (i) As in h, but with SA-induced SGs. ***, P < 0.001; *, P < 0.05; one-way ANOVA, Bonferroni post-hoc test. Bars: (main panels) 10 µm; (a, d, and g, insets) 2 µm.

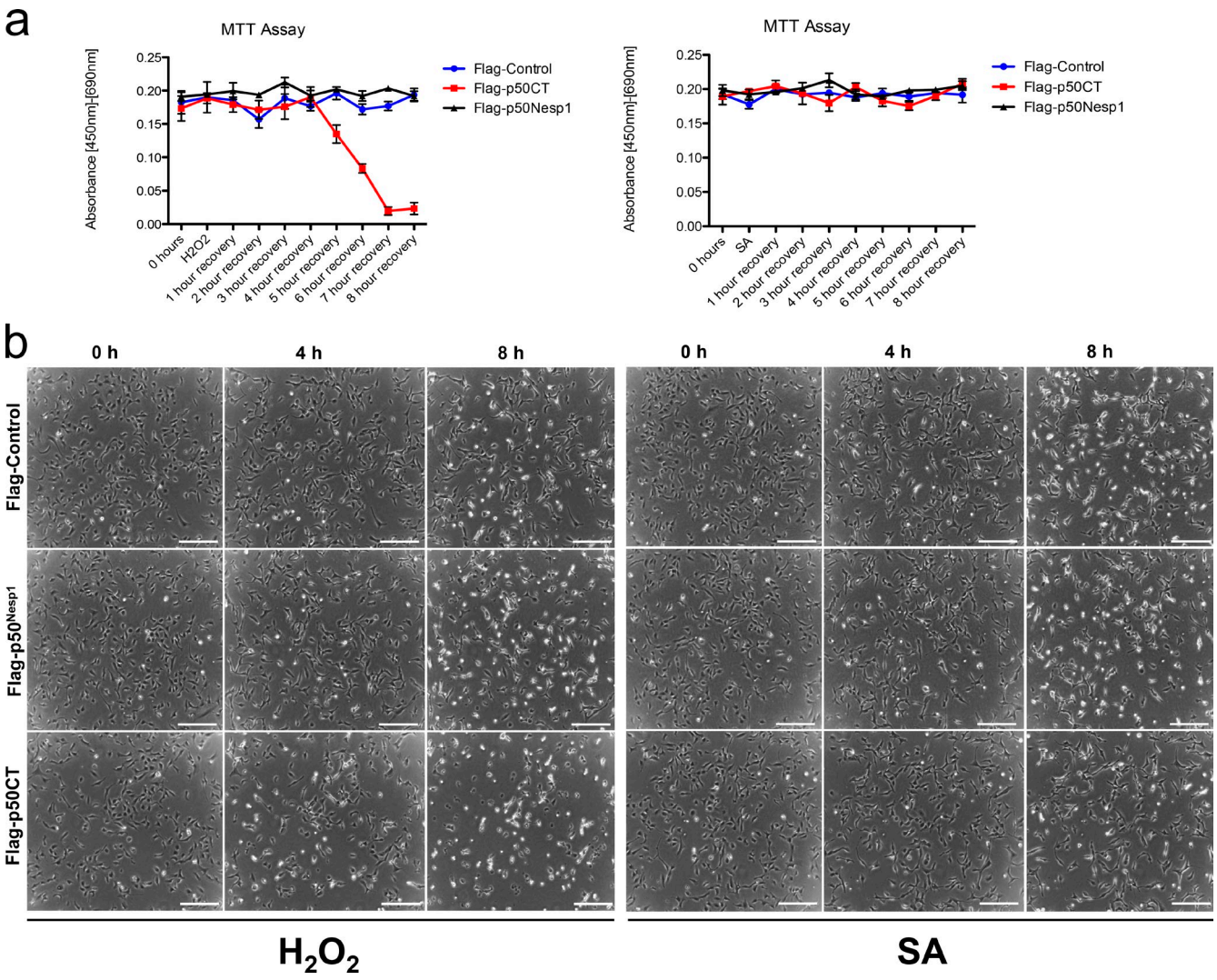


Figure 7. **Flag-p50CT promotes cell death in response to $H_2O_2$.** (a) Cells were treated with $H_2O_2$ or SA for 1 h to induce SGs, followed by hourly MTT readings during recovery. 0 h is MTT reading before stress. (b) Time-lapse microscopy demonstrates lethality of Flag-p50CT in U2OS cells ~8 h after $H_2O_2$ stress relief, but not after SA. Bars, 10 µm.

region of these proteins to SR1+2 of p50$^{Nesp1}$ (Fig. 10). These interactions with p50$^{Nesp1}$ were RNA dependent; however, we do not know if RNA can interact directly with SR1+2 or whether they are bridged by other RNA-binding proteins to p50$^{Nesp1}$.

In U2OS cells, Flag-p50$^{Nesp1}$ promoted MT bundling and was able to bind MTs in vitro through SR3+4 (p50CT). By interacting with PB components via SR1+2 and possessing MT-binding domains in SR3+4, we show p50$^{Nesp1}$ is a PB–MT linker. In support of this, Flag-p50$^{Nesp1}$ recruited Rck/p54 to bundled MTs, whereas Flag-p50CT de-coupled Rck/p54 from MTs by acting as a dominant negative.

Interestingly, no GW182 was initially detected as binding to p50$^{Nesp1}$. However, GW182 localized to MTs in Flag-p50$^{Nesp1}$– and Flag-p50CT–transfected U2OS cells, suggesting the two proteins may interact in an MT-dependent manner. Indeed, GW182 was detected in pAb4 co-IPs and with GST-p50$^{Nesp1}$ and GST-p50CT in the presence of taxol.

Unlike U2OS cells, in VSMCs, which express fewer PBs, Flag-p50$^{Nesp1}$ localized to and induced PB formation. These different localizations were not simply due to differences in expression levels of the construct between the cell lines, as U2OS cells expressing low levels of Flag-p50$^{Nesp1}$ also showed MT localization (unpublished data). Rather, we provide evidence that the differences in localization may be due to the abundance of other PB components associated with p50$^{Nesp1}$. We showed that VSMCs express more Dcp1a, Ago2, and Rck/p54, but not GW182, compared with U2OS cells, and that Flag-p50$^{Nesp1}$ co-expressed with Dcp1a-YFP in U2OS cells preferentially colocalized with Dcp1a-YFP PBs and not to MTs. This contrasted with Flag-p50CT, which remained attached to MTs when coexpressed with Dcp1a-YFP. Furthermore, although Flag-p50CT also localized to MTs in VSMCs, Flag-p50$^{Nesp1}$ relocalized from PBs to MTs when Dcp1a RNAi was performed. Taken together, these data suggest that the abundance and/or stoichiometry of proteins bound to SR1+2 of p50$^{Nesp1}$ influence whether it localizes to PBs or MTs. We also observed that Flag-p50$^{Nesp1}$ overexpression in U2OS increased levels of Dcp1a and other N-terminal binding partners, suggesting that a feedback mechanism regulates

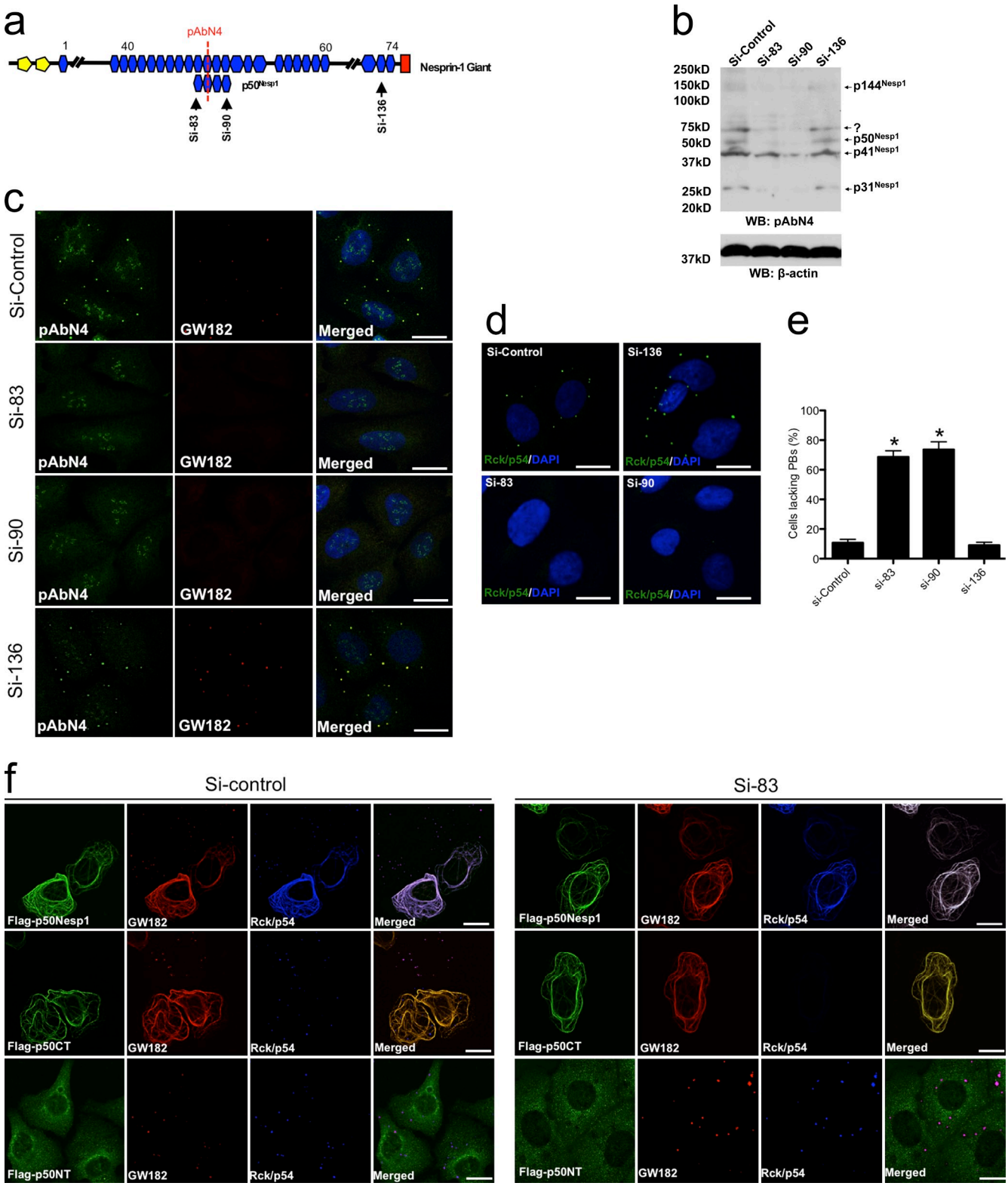


Figure 8. **p50$^{Nesp1}$ knockdown eliminates PBs.** (a) Schematic depicting siRNA oligos relative to nesprin-1 giant and p50$^{Nesp1}$. (b) Immunoblotting confirmed efficiency of si-83 and si-90 RNAi. (c) si-83– and si-90–mediated p50$^{Nesp1}$ RNAi eliminates pAbN4 and GW182 PBs in U2OS cells. (d) si-83 and si-90 eliminates Rck/p54 PBs. (d) Quantification of PB depletion in U2OS cells ($n$ = 600 cells). *, $P < 0.001$; one-way ANOVA, Dunnett's post-hoc test. (f) Flag-p50$^{Nesp1}$, Flag-p50NT, and Flag-p50CT rescues in si-83–transfected cells. Bars, 10 µM.

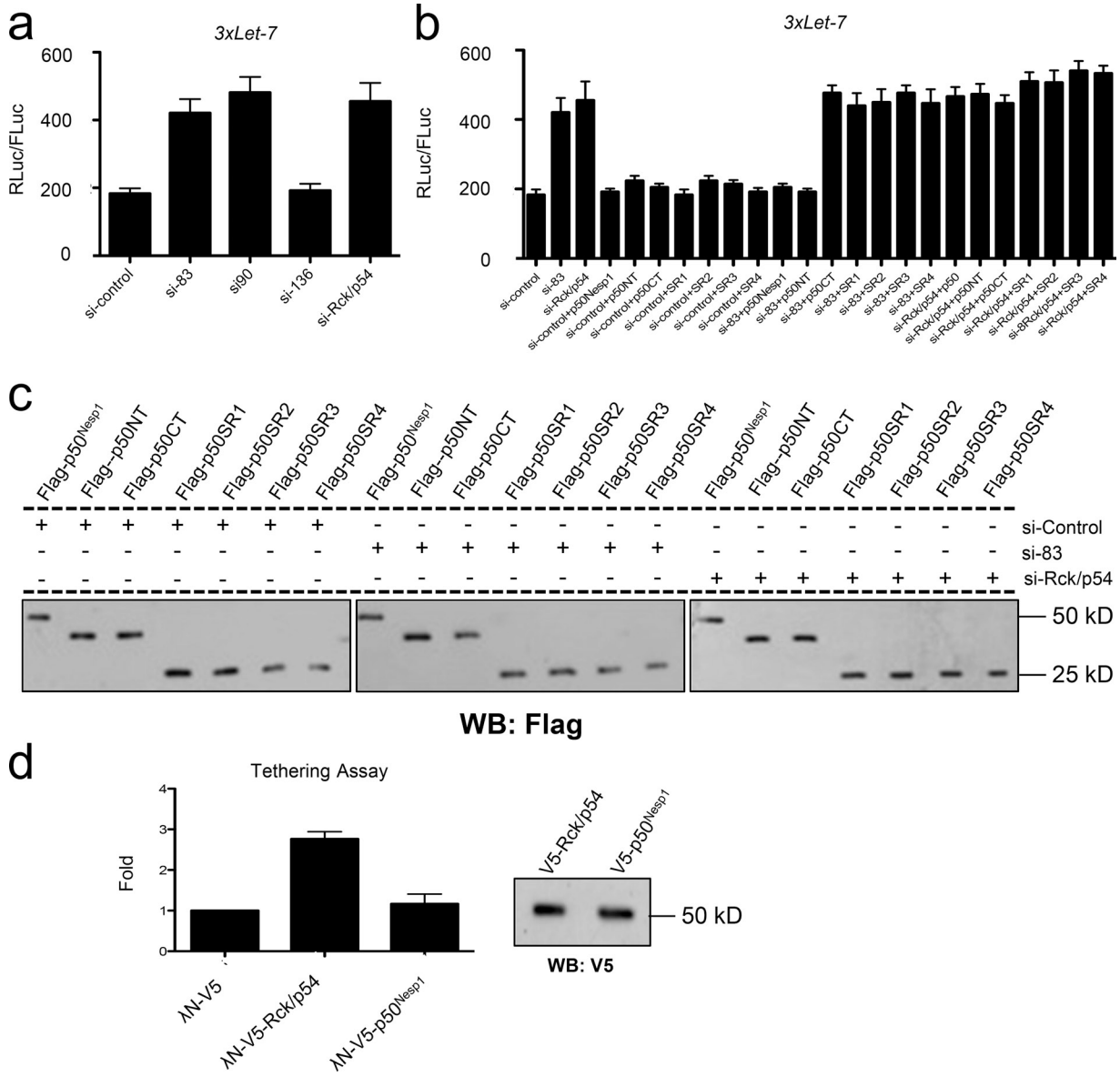


Figure 9. **p50$^{Nesp1}$ is required for miRISC function.** (a) Cells depleted of p50$^{Nesp1}$ have attenuated miRISC function. si-Rck/p54 served as a positive control. (b) Flag-p50$^{Nesp1}$ and Flag-p50NT rescued si-83 miRISC in U2OS cells. (c) Immunoblotting shows expression levels of nesprin constructs in RNAi cells. (d) Tethering λN-V5-p50$^{Nesp1}$ to 5BoxB sites present in the 3′UTR of *Renilla* had no effect on silencing. λN-V5-Rck/p54 served as positive control. Immunoblots show expression levels of p50$^{Nesp1}$ and Rck/p54.

the abundance of these binding partners. This is also supported by the observation that Flag-p50CT did not increase levels of the binding partners. Unfortunately, due to the poor transfection efficiency of VSMCs, we were unable to test this further and future studies using constructs cloned into viral vectors are needed. Whether additional proteins also operate within this complex to regulate PB versus MT association also needs to be determined.

We showed the SRs in p50CT directly interact with MTs in tandem but also appear to promote MT bundling. This bundling is potentially due to recruitment of MT cross-linkers and further screening of p50$^{Nesp1}$-binding partners may identify such factors. As high levels of Dcp1a appeared to attenuate MT bundling, proteins bound to the SRs in p50NT may play a role. Alternatively, bundling may be achieved by oligomerization of p50$^{Nesp1}$. Dimerization of SR proteins is not uncommon and both nesprin-1α and nesprin-3α have been shown to dimerize in vitro (Djinovic-Carugo et al., 2002; Mislow et al., 2002; Ketema et al., 2007). In addition, protein regulator of cytokinesis 1 (PRC1, also known as MAP65) interacts directly with MTs via its SRs to bundle anti-parallel filaments by forming homodimers produced from opposing centrioles (Subramanian et al., 2010). Whether p50$^{Nesp1}$ can cross-link MT filaments into bundles by forming such homodimers is worth further exploration.

### p50$^{Nesp1}$ is a core miRISC protein

We identified p50$^{Nesp1}$ as a scaffold for miRISC complexes based on its ability to interact with Rck/p54, Ago2, and GW182. p50$^{Nesp1}$ knockdown attenuated miRISC activity, leading to PB elimination in U2OS cells. Importantly, VSMCs also showed attenuated miRISC activity and reduced PB numbers when

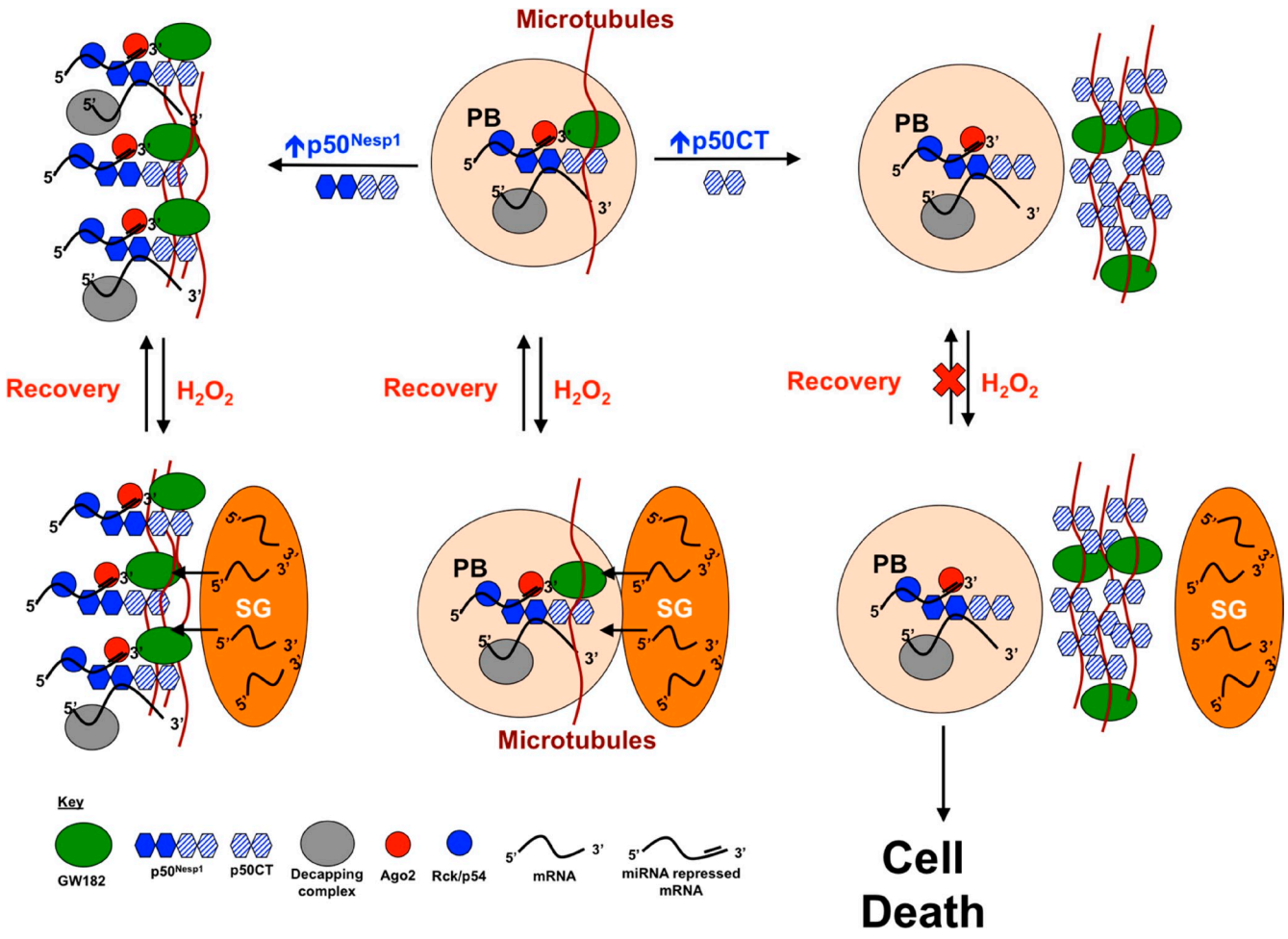


Figure 10. **p50$^{Nesp1}$ functions in PB and SG dynamics.** SR1+2 of p50$^{Nesp1}$ (blue hexagons) interact with Ago2, Rck/p54, and Dcp1a in an RNA-dependent manner and SR3+4 (blue and white dashed line hexagons) of p50$^{Nesp1}$ interact in an MT-dependent manner with GW182. $H_2O_2$ induces SGs, which associate with PBs in an MT-dependent manner. Upon recovery, SGs disassemble and normal RNA control is resumed. p50CT overexpression promotes MT bundling and displaces endogenous p50$^{Nesp1}$ PBs from MTs, but does not remove GW182 from MTs. In p50CT-overexpressing cells, $H_2O_2$-induced SGs do not associate or cross talk with MT-detached PBs, hampering sorting and disassembly, leading to cell death. In contrast, when p50$^{Nesp1}$ is overexpressed, MT filaments bundle and mRNPs attached to p50$^{Nesp1}$ are recruited to MTs. In these cells, association and cross talk between p50$^{Nesp1}$-associated mRNPs and SGs occurs and SGs disassemble.

transfected with si-83 and si-90, but not si-136, suggesting both cell lines have similar p50$^{Nesp1}$ miRISC functionality (unpublished data). Rescue experiments in U2OS cells demonstrated these effects were most likely caused by p50$^{Nesp1}$ knockdown and not other isoforms targeted by the siRNAs. p50$^{Nesp1}$ rescue restored miRNA function; however, p31$^{Nesp1}$, which was knocked down by si-83 and si-90 RNAi and did not interact with PB components, was unable to rescue miRISC despite containing p50NT SRs. Although we cannot rule out the possibility that another larger unidentified isoform also depleted by both siRNAs plays a role in PB biology, this evidence suggests that each nesprin-1 isoform has unique localization and binding properties that potentially restrict its functionality to a particular process.

p50$^{Nesp1}$ rescue recruited Rck/p54 and GW182 to MTs, demonstrating PB components recruited to MTs have functional miRISCs. p50CT rescue did not restore miRISC activity; however, it was able to restore GW182 to MTs, indicating GW182 bound to MTs alone cannot function in silencing. Likewise, Flag-p50CT could not attenuate miRISC activity in control cells, suggesting p50$^{Nesp1}$ links to MTs are not critical for miRISC function. Although the dynamics of p50$^{Nesp1}$–GW182 interactions on MTs require further investigation, we speculate that MT filaments may transiently bring GW182 into close proximity with the mRNPs bound to SR1+2 to mediate miRNA-mediated gene silencing. However, p50NT was also able to rescue miRISC activity to the same extent as full-length p50$^{Nesp1}$, and interestingly, restored Rck/p54 and GW182 PBs without localizing to PBs itself. Potentially, small amounts of p50NT may be present within the restored PBs and account for miRISC rescue. Alternatively, silencing may occur in the cytosol rather than PBs, as miRISC silencing has been shown to occur in the absence of PBs (Chu and Rana, 2006; Eulalio et al., 2007b). The reestablishment of GW182 was surprising, considering it is unable to interact with p50NT. It is plausible the revival of Rck/p54 (and likely Ago2) may change the organization or conformations of mRNPs within the newly formed PBs, for example, by allowing GW182 to form direct interactions with Rck/p54 and Ago2 attached to the SRs of p50NT.

Interestingly, $p50^{Nesp1}$ alone was unable to induce silencing when tethered to a reporter mRNA construct, suggesting it needs to associate with GW182 complexes to induce silencing. These associations could be transient and mediated by MTs; however, the factors regulating such interactions remain unclear. For example, GW182 may interact independently with MTs via other mechanisms such as Myosin-Va (see below) or other linker proteins that mediate nesprin–GW182 interactions. These possibilities require further investigation.

### $p50^{Nesp1}$ regulates PB motion

By de-coupling endogenous $p50^{Nesp1}$ PB–MT links with Flag-p50CT, Dcp1a-YFP movement was significantly reduced. Dcp1a-YFP motion in these cells was similar to Flag-control cells treated with nocodazole, suggesting the reduced PB motion in Flag-p50CT cells is due to displacement of endogenous $p50^{Nesp1}$ complexes from MTs rather than the retention of GW182 to MTs or the separation of GW182 from other proteins bound to SR1+2 of $p50^{Nesp1}$. Myosin-Va has previously been shown to be required for PB motion and is known to move along MTs in association with kinesins (Huang et al., 1999; Wu et al., 2005; Hodges et al., 2009; Lindsay and McCaffrey, 2011), and when Dcp1a PBs were tracked in cells expressing dominant-negative Myosin-Va, reduced PB movements were observed to similar levels as cells expressing Flag-p50CT in our experiments. However, Myosin-Va does not interact with the $p50^{Nesp1}$–binding partner Dcp1a, indicating multiple MT linker proteins are present in PBs and may act to promote mRNP-specific attachments.

### PB–SG dynamics are dependent on PBs being associated with MTs

During stress, SGs form as an adaptive mechanism to provide protection against apoptosis (Arimoto et al., 2008). SGs and PBs have different dynamic properties in size, shape, and movement. SGs are relatively static but able to change shape, fuse, and divide. By contrast, PBs are mobile and tend not to change their size or spherical shape (Moser and Fritzler, 2010). Therefore, PB–SG cross talk is likely to be dependent on MT PB-mediated collisions with SGs. Previously, PBs and SGs lost connections in nocodazole-treated cells (Aizer et al., 2008). Here, we demonstrate that by leaving MTs intact, but detaching PBs from them using Flag-p50CT, PB–SG cross talk is impaired. This finding indicates that PB–SG connections are dependent on PBs being attached to MTs, which presumably allow PBs to probe a greater cytoplasmic volume for locating SGs.

Interestingly, $H_2O_2$-induced SGs, but not SA-induced SGs, failed to dissolve in Flag-p50CT cells. Recently, the Anderson group showed $H_2O_2$-induced SGs assemble independently of the phosphorylation of eIF2α, a major trigger of SG assembly used by common stressors such as SA. Additionally, they demonstrated $H_2O_2$-induced SGs are compositionally distinct from canonical SGs (Emara et al., 2012). To date, SG disassembly mechanisms remain poorly characterized, and our study suggests canonical SGs and $H_2O_2$-induced SGs are likely to have different disassembly pathways. For $H_2O_2$-induced SGs, but not canonical SGs, we propose a model where connections with PBs are essential for the transferal of specific cues or stimuli from or to PBs during stress that provide disassembly signals during recovery.

The hampered SG dynamics in Flag-p50CT cells could also be due to the separation of GW182 from proteins bound to SR1+2 of $p50^{Nesp1}$. When all factors were retained at MTs in Flag-$p50^{Nesp1}$ cells, SGs were in close proximity to Rck/p54 MTs and the β-globin reporter was present throughout the MTs, with ∼30% of all SGs containing some reporter. Although this was significantly higher than the ∼20% of β-globin containing SGs in Flag-control cells, it was markedly lower than the ∼90% of SGs in Flag-p50CT cells where SG–PB communication was clearly impaired. Thus, displacement of $p50^{Nesp1}$ N-terminal binding partners from MTs and GW182 drastically impairs mRNA sorting. Furthermore, $H_2O_2$-induced SGs in Flag-$p50^{Nesp1}$ cells disassembled in recovery, indicating mRNPs retained on MTs do not affect SG disassembly, and their failure to dissolve in Flag-p50CT cells is also due to displacement of N-terminal $p50^{Nesp1}$ binding partners from MTs and GW182. Whether these hampered dynamics are due to separation of GW182 from the N-terminal binding partners, detachment of binding partners from MTs, or a combination of both still warrants further investigation.

Moreover, Flag-p50CT–expressing U2OS cells exhibit irreversible cellular cytotoxicity resulting in cell death once exposed to $H_2O_2$. We speculate their inability to transfer mRNPs to PBs for degradation or storage during stress and recovery hampers mRNA sorting, resulting in global shutdown of translation. In turn, this could result in a deficiency of repair enzymes synthesized to deal with the $H_2O_2$-induced damage. The cell death observed in Flag-p50CT cells is likely to be specific to PB–SG disruptions as a result of $H_2O_2$ exposure, as Flag-control and Flag-$p50^{Nesp1}$ cells were viable under the same conditions, as were Flag-p50CT cells exposed to SA. Whether other forms of stress such as heat shock, glucose deprivation, and UV exposure trigger cell death when PBs are detached from MTs would also be worth exploring. Furthermore, it will be interesting to determine whether the cell death induced by $H_2O_2$ is specific for U2OS cells. Due to the poor transfection efficiency this could not be tested in HDFs and VSMCs; however, future studies should look at examining this phenomena in other cell types.

### Other nesprin-1 MAP variants

$p50^{Nesp1}$ terminates with the N1-3′E90 3′UTR, and therefore all isoforms ending with this UTR will contain the two MT-binding SRs at their C termini. These variants are likely to be expressed in a tissue-specific manner and scaffold-specialized protein complexes and/or organelles to the MT cytoskeleton.

Previously, two nesprin-1 mutations causing premature terminations (306434A>G and 310067A>G) were identified in patients with autosomal-recessive cerebellar ataxia type 1 that would disrupt nesprin-1 MAP variants (Gros-Louis et al., 2007). Moreover, mutations in other PB components have also been described in neurodegenerative diseases. For example, the Huntington protein mutated in Huntington's disease was identified as an Ago2-binding protein, and like $p50^{Nesp1}$ localizes to PBs and is necessary for their formation and silencing function (Savas et al., 2008). Furthermore, Ataxin-2 is mutated in spinocerebellar

ataxia type 2 and interacts with Rck/p54 and localizes to both PBs and SGs (Affaitati et al., 2001; Nonhoff et al., 2007). Therefore, disruption of nesprin-1 MT scaffolds promoting defects in PB assembly, motion, silencing functions, and SG cross talk in the neuronal system could be a novel casual occurrence promoting neurological diseases.

## Materials and methods

### Plasmids

Flag-p50$^{Nesp1}$ and Flag-p31$^{Nesp1}$ were previously cloned by our laboratory (Rajgor et al., 2012). Both transcripts were *Taq* PCR amplified from tissue cDNA and cloned into pGEM-T Easy. The pGEM-T plasmids were subsequently used as templates for *Pfu* amplification with primers containing EcoRV and Xho1 restriction sites and ligated into pCMV-Tag2 vector harboring an N-terminal Flag-tag. Flag-p50NT, -p50CT, -p50SR1, -p50SR2, -p50SR3, and -p50SR4 were cloned from Flag-p50$^{Nesp1}$ as a template using *Pfu polymerase* (Promega) and specific primers containing the EcoRV and Xho1 restriction sites Flag-p50NT (forward: 5′-GATATCATGCAGGAGAAAGTGAAGACT-3′; reverse: 5′-CTCGAGTCACTGATGCAAAATATATTGT-3′), Flag-p50CT (forward: 5′-GATATCATGACCCTGCTAGAAGAATCCAAA-3′; reverse: 5′-CTCGAGCTACTGGTGTGGGTACCCTG-3′), Flag-p50SR1 (forward: 5′-GATATCATGCAGGAGAAAGTGAAGACT-3′; reverse: 5′-CTCGAGTCAGCCTTGCTCTGCTCAACTTCT-3′), Flag-p50SR2 (forward: 5′-GATATCACGAGCCAGGAACTCAGCC-3′; reverse: 5′-CTCGAGTCACTGATTGAGCTTGGAGAGCCG-3′), Flag-p50SR3 (forward: 5′-GATATCGCAGCATCACATTTAGAAG-3′; reverse: 5′-CTCGAGTCAATCCTTAGCTGCATCTTGGA-3′), and Flag-p50SR4 (forward: 5′-GATATCTGAAAAAATTTGAAGCAG-3′; reverse: 5′-CTCGAGCTACTGGTGTGGGTACCCTG-3′). The PCR products were subcloned into pGEM-T Easy (Promega), digested with EcoRv and XhoI, and ligated into the complementary sites of Flag-tag vector pCMV-Tag2 (Takara Bio Inc.). The GST constructs were cloned into pGEX-4T-3 by PCR amplification off their respective Flag variants in a similar fashion using primers with Sma1 and Xho1 restriction sites GST-p50$^{Nesp1}$ (forward: 5′-CCCGGGATGCAGGAGAAAGTGAAGACT-3′; reverse: 5′-CTCGAGTCACAGGGTACCCACACCAGTAGCTCGAG-3′), GST-p50NT (forward: 5′-CCCGGGATGCAGGAGAAAGTGAAGACT-3′; reverse: 5′-CTCGAGTCACTGATGCAAAATATATTGT-3′), GST-p50CT (forward: 5′-CCCGGGATGACCCTGCTAGAAGAATCCAAA-3′; reverse: 5′-CTCGAGCTACTGGTGTGGGTACCCTG-3′), GST-p50SR1 (forward: 5′-CCCGGGATGCAGGAGAAAGTGAAGACT-3′; reverse: 5′-CTCGAGTCAGCCTTGCTCTGCTCAACTTCT-3′), GST-p50SR2 (forward: 5′-CCCGGGACGAGCCAGGAACTCAGCC-3′; reverse: 5′-CTCGAGTCACTGATTGAGCTTGGAGAGCCG-3′), GST-p50SR3 (forward: 5′-CCCGGGGCAGCATCACATTTAGAAG-3′; reverse: 5′-CTCGAGTCAATCCTTAGCTGCATCTTGGA-3′), and GST-p50SR4 (forward: 5′-CCCGGGATGAAAAAATTTGAAGCAG-3′; reverse: 5′-CTCGAGCTACTGGTGTGGGTACCCTG-3′).

pEYFP-Dcp1, pEF-7B-MS2bs, and pEGFP-MS2 were gifts from N. Kedersha (Harvard University, Boston, MA; Kedersha et al., 2005). pEGFP-GW182 was a gift from M. Fritzler (University of Calgary, Alberta, Canada; Eystathioy et al., 2002). pDsRed2-C1-Rck/p54 was provided by N. Standart (Cambridge University, Cambridge, England, UK; Minshall et al., 2009). Vectors psi-CHECK2-let-7X3 and psi-CHECK2-let-7X3m were provided by G. Hutvagner (University of Dundee, Scotland, UK; Johnston et al., 2010). pRK5-Myc-PSK1a was a gift from J. Morris (King's College London, London, England, UK; Mitsopoulos et al., 2003).

### Tissue culture

Human dermal fibroblasts (HDFs), osteosarcoma cells (U2OS), and C2C12 myoblasts were passaged after reaching 70% confluency and maintained in DMEM complete media (Sigma-Aldrich) supplemented with 10 U/ml penicillin, 10 mg/ml streptomycin, 200 µM L-glutamine, and 10% FBS. Primary or SV40 VSMCs were cultured in medium M199 (Sigma-Aldrich) supplemented in 10 U/ml penicillin, 10 mg/ml streptomycin, 200 µM L-glutamine, and 20% FBS. When appropriate, cells were treated with 10 µg/ml nocodazole, 10 µg/ml cycloheximide, 500 µM sodium arsenite, or 2 µM $H_2O_2$ for 1 h.

### Generation of nesprin-1 pAbN4 and pAbN5

Polyclonal rabbit antibodies to human nesprin-1 N4 and N5 were generated against synthetic polypeptides EQNGQLGKPLAKKIGKL and QTIRQAENRLSKLNQA, respectively (residues 5488–5504 and 5510–5525, respectively, of nesprin-1 giant; Immune Systems Ltd). Although the N4 and N5 sequences are located within SR49 of nesprin-1, a BLAST search of public protein databases failed to identify significant homology to any other nesprin family members or SR proteins, supporting their specificity for nesprin-1. Immune Systems Ltd. synthesized and conjugated the N4 and N5 epitope peptide to keyhole limpet hemocyanin and injected these complexes individually into rabbits to generate polyclonal antibody sera. The immune sera were affinity purified against peptide columns to isolate the antibodies of interest.

### Immunoblotting

Whole-cell lysates were prepared by scraping PBS-washed cells in ice-cold co-IP buffer (10 mM Tris, pH 7.4, 150 mM KCl, 1 mM EDTA, 1% Triton, and protease inhibitor cocktail). Lysed cells were centrifuged at 13,050 *g* for 20 min to obtain the supernatant lysate, and up to 20 µg of lysate were resolved on a 10% SDS-PAGE gel and transferred to PVDF using a semi-dry apparatus. The membranes were blotted with the antibodies indicated in each figure, and bands were visualized using the ECL Western blotting substrate (Thermo Fisher Scientific). Membranes were incubated with the following primary antibodies at a 1:1,000 dilution: rabbit polyclonal pAbN4, rabbit polyclonal pAbN5, mouse monoclonal anti-Rck/p54 (ab54611; Abcam), mouse monoclonal anti-Ago2 (ab57113; Abcam), mouse monoclonal anti-Dcp1a (ab57654; Abcam), rabbit polyclonal anti-Rck/p54 (A300-461A; Bethyl Laboratories, Inc.), mouse monoclonal anti-Flag (F3165; Sigma-Aldrich), and anti-GAPDH (sc-365062; Santa Cruz Biotechnology, Inc.). Mouse monoclonal anti–β-actin (A-9452; Sigma-Aldrich), mouse anti–α-tubulin (T5168; Sigma-Aldrich), and goat polyclonal anti-GST (ab6613; Abcam) were used at 1:10,000. Mouse monoclonal anti-GW182 4B6 (sc-56314; Santa Cruz Biotechnology, Inc.) was diluted 1:10. The following antibodies were used at 1:500: rabbit polyclonal anti-Ago2 (ab135025; Abcam) and rabbit anti-Dcp1a (ab47811; Abcam). Secondary antibodies conjugated to HRP were obtained from GE Healthcare and used at 1:10,000 dilutions.

### Let-7 miRISC luciferase assay

12,000 U2OS cells were plated into each well of a 24-well plate and cultured under standard growth conditions overnight. The following day, three wells per experimental condition were transfected with 1 µl nesprin or Rck/p54 or scrambled siRNA oligos (all at 20-µM stock solutions) using HiPerFect (QIAGEN) transfection reagent. 72 h after siRNA transfection, 1 µg of psi-CHECK2-let-7X3 or psi-CHECK2-let-7X3m was cotransfected with Flag constructs into each well using SuperFect (QIAGEN) transfection reagent. Luciferase readings were taken 24 h after plasmid transfection using the Dual-Luciferase Reporter assay (Promega). *Renilla* luciferase activity was normalized to *FireFly* luciferase activity to control for transfection efficiency (both transcribed off the psi-CHECK2 plasmids).

### Plasmid transfections

Plasmids were transfected into U2OS cells, HDFs, and VSMCs using SuperFect transfection reagent (QIAGEN) according to the manufacturer's instructions. Cells were transfected onto coverslips or MatTek glass-bottom dishes and fixed for immunostaining or used for time-lapse microscopy 24 h after transfection, respectively.

### Tethering assay

50,000 U2OS cells were plated per well of a 6-well plate and transfected with 1 µg phRL-Gl-5BoxB, 1 µg of pCI-neo-lambdaN-V5, and 50 ng pGL3 using SuperFect transfection reagent the following day. 48 h after transfection, luciferase readings were taken using the Dual-Luciferase reporter assay system.

### Immunofluorescence microscopy

Cells were fixed for 5 min in 3.7% PFA (Sigma-Aldrich) followed by 2 min permeabilization with 0.5% NP-40 (EMD Millipore). The coverslips were incubated with blocking solution (1% BSA) for 1 h at RT. Primary antibodies used for immunostaining were diluted in blocking solution and applied to the coverslips for 1 h at RT followed by three short rinses in PBS. Primary antibodies were as follows: rabbit anti-pAbN4 was diluted at 1:100, rabbit anti-pAbN5 at 1:100, goat anti-eIF3η (sc-16377; Santa Cruz Biotechnology, Inc.) at 1:100, mouse anti-PABP-1 (10E10, sc-32318; Santa Cruz Biotechnology, Inc.) at 1:200, mouse anti–c-myc (sc-40; Santa Cruz Biotechnology, Inc.) at 1:200, mouse anti-S6K used to detected Hedls (sc-8418; Santa Cruz Biotechnology, Inc.) at 1:200, rabbit anti-Rck/p54 (A300-461A; Bethyl Laboratories, Inc.) at 1:200, mouse anti-Flag M2 (F1804; Sigma-Aldrich) at 1:1,000, mouse anti-fibrillarin (ab4566; Abcam) at 1:500, mouse anti–α-tubulin (T5168; Sigma-Aldrich) at 1:1,000, polyclonal rabbit anti-Flag (F7425; Sigma-Aldrich) at 1:500, mouse anti-Flag

(F3165; Sigma-Aldrich) at 1:1,000, goat anti-Flag (ab1257; Abcam) at 1:300, and anti-GW182 4B6 (sc-56314; Santa Cruz Biotechnology, Inc.) at 1:5. Next, the coverslips were incubated with secondary antibodies, diluted 1:1,000 in blocking buffer, conjugated to Alexa Fluor 405, 488, or 546 (Invitrogen) for 1 h at RT. The coverslips were next stained with DAPI and washed with PBS before being mounted onto slides using Mowiol mounting media. Images were acquired at room temperature using either confocal or conventional microscopy. For confocal microscopy, images were acquired using a confocal microscope (model SP5; Leica) under a 63×/1.4 NA oil-immersion objective. The Leica application suite software was used to acquire 0.37-µm stepped Z-stacks throughout the depth of the cells, and maximal intensity projections generated by the Leica application suite software are presented within this manuscript. For conventional microscopy, images were acquired using a cooled CCD camera (Orca-R2; Hamamatsu Photonics) attached to a wide-field microscope (model IX81; Olympus) with a 40× LCUPlanFLN/0.6 NA air objective, and acquisition was controlled using Volocity software (PerkinElmer).

**Peptide blocking**

For peptide-blocking experiments, blocking peptides were designed to the antibody epitope of interest and synthesized by Peptide Protein Research Ltd. 10 µg of peptide was incubated with every 1 µg of primary antibody diluted in 1% BSA blocking buffer. For pAbN4 peptide blocking, the pAbN5 peptide served as a control and vice versa. The mixture was incubated with constant rotation for 1 h at RT and then incubated with fixed cells on coverslips for 1 h at RT. The ability of the peptide to block staining was determined by immunofluorescence microscopy.

**Time-lapse microscopy**

For PB tracking, U2OS cells were transfected as described with appropriate constructs in phenol red–free DMEM and imaged on a microscope (model IX81; Olympus) with a 40× LCUPlanFLN/0.6 NA air objective with additional intermediate magnification of 1.6, giving a total magnification of 64. Volocity was used to control time-lapse acquisition and images were acquired every 200 ms for 2 min using a cooled CCD camera (Orca-R2; Hamamatsu Photonics) set to 2 × 2 binning (effective pixel size of 0.21 µm/pixel) and with an exposure of 30 ms. Image stacks were deconvolved in Volocity using the "fast" (noniterative) method. PBs were detected using an intensity threshold of at least three standard deviations from the mean of whole image intensity, with a minimum object area of 0.5 $\mu m^2$, and using a 4-µm local contrast adjustment. Resultant objects were dilated by 1 pixel and subject to a 3 × 3-pixel Gaussian filter to remove noise. Touching objects were separated by giving Volocity a size guide of 5 $\mu m^2$. Dcp1a-YFP bodies were tracked using a "shortest path" algorithm with a maximum distance of 1 µm between frames. The area centroid of each tracked object was exported as a list of coordinates and converted to CEL format in a custom-written Mathematica (Wolfram Research) notebook, and CEL files were imported into the Chemotaxis Analysis notebook v1.6 (Graham Dunn, King's College London, London, England, UK) for analysis and statistical comparison.

For monitoring cell death, U2OS cells were transfected with the relevant constructs in 6-well plates and imaged on the same microscope and camera with a 10×/0.3 NA air objective. Three separate points were identified for filming per well, and Volocity was used to acquire images with 15-ms exposures every 2 min over a 16-h time frame.

**Transmission immunoelectron microscopy**

Cells were seeded onto 35-mm culture dishes 24 h before harvest. At the time of harvest, the cells were fixed in 100% methanol at 4°C for 10 min. The preparation was then washed in PBS and incubated with the pAbN4 antibody (diluted 1:200) at room temperature for 30 min. Subsequently, the preparations were washed three times with PBS and then incubated for 40 min with protein A gold (Polysciences). The preparations were then washed three times in PBS, post-fixed in 2% glutaraldehyde for 1 h, passed through a graded ethanol series, and embedded in Epon 812 (Polysciences). After polymerization, the material was sectioned in an ultramicrotome (Leica) equipped with a diamond knife, and sections were stained with uranyl acetate and lead citrate and examined under a transmission electron microscope (model H7650; Hitachi) operated at 80 kV with a 50-µm objective aperture, and images were taken with a digital camera (model 16000; AMT Corp.) mounted on the microscope.

**MTT assay**

In vitro toxicity was measured using an MTT (3-[4,5-dimethylthiazol-2-yl]-2,5-diphenyl tetrazolium bromide)-based assay. Transfected cells were cultured in media supplemented with 10% MTT reagent for 3 h. Next, the culture was aspirated off and the resulting formazan crystals were dissolved in MTT solubilization solution, equal to the original culture medium volume. The 96-well plate was then placed on a shaker for 10 min to enhance the dissolution of the crystals and spectrophotometrically measures were taken at 570-nm and 690-nm absorbances. 690-nm readings were subtracted from 570-nm readings to eliminate background.

**Co-immunoprecipitations**

co-IPs were performed on U2OS whole-cell lysates. Cells were washed with PBS and extracts were prepared by scraping cells in ice-cold co-IP buffer (10 mM Tris, pH 7.4, 150 mM KCl, 1 mM EDTA, 1% Triton, and protease inhibitor cocktail). For the more stringent conditions used to detect GW182 in pAbN4, Ago2, Dcp1a, and Rck/p54 immune complexes, co-IP buffer containing 250 mM KCl was used. Lysed cells were centrifuged at 13,050 *g* for 20 min to obtain the supernatant lysate, which was precleared with Protein A– or Protein G–Sepharose beads (Sigma-Aldrich) for 1 h at 4°C with rotation. Protein complexes were obtained by incubating 2 µg of relevant antibody with 200 µg of cell lysate overnight at 4°C with gentle rotation. Immune complexes were purified using Sepharose beads, washed three times with co-IP buffer, boiled in loading buffer, and analyzed by immunoblotting.

The co-IPs for the RNase treatment were performed under identical conditions. However, washed beads were resuspended into co-IP buffer and divided into two equal volumes. 10 µg/ml RNase mixture (DNase free; Roche) was added to one, and both were incubated at room temperature for 20 min. After two washes in cold co-IP buffer, proteins were eluted in loading buffer.

Cells used for co-IPs to be performed in MT-stabilized cells were incubated for 24 h with 20 nM paclitaxel (taxol) before being lysed in co-IP buffer supplemented with 20 nM taxol. Cells used for co-IPs to be performed in MT-depolymerized cells were incubated for 1 h with 10 µg/ml nocodazole before being lysed in co-IP buffer supplemented with 10 µg/ml nocodazole.

**GST pull-downs**

GST and GST fusion proteins were induced from 100 ml of bacterial culture for 2 h using 0.2 mM IPTG (Sigma-Aldrich) at 30°C. Purification of the proteins was performed according to the GE Healthcare protocol using glutathione-Sepharose 4B beads (GE Healthcare). Pull-downs were performed from U2OS whole-cell lysates prepared as described above. 200 µg of protein lysates were incubated with 30-µl beads overnight at 4°C with rotation. Bound proteins were eluted into protein loading buffer and immunoblotting was performed. Pull-downs to be performed in MT-stabilized cells were incubated for 24 h with 20 nM paclitaxel (taxol) before being lysed in co-IP buffer supplemented with 20 nM taxol.

**Microtubule sedimentation assays**

In vitro microtubule-binding assays were performed using the Microtubule Binding Protein Spin-Down Assay kit (BK029; Cytoskeleton, Inc.). GST-purified proteins were prepared as described above and incubated with polymerized microtubules in an Eppendorf tube according to the manufacturer's instructions. In brief, microtubules were assembled in Eppendorfs by incubating tubulin protein with a cushion buffer for 20 min at 35°C. After assembly, a tubulin buffer containing taxol was added to the microtubules to maintain their stability for several hours at RT. Next, 5 µg of GST-purified proteins were incubated with microtubules for 30 min at RT followed by ultracentrifugation at 100,000 *g* for 40 min at RT. The supernatant containing the unbound fraction was carefully placed into an additional Eppendorf and the pelleted microtubules were resuspended into protein loading buffer with β-mercaptoethanol. The two fractions were analyzed by immunoblotting using anti-GST antibody.

**Online supplementary methods**

Figs. 5 (A and B), 6 (A, D, and G), and 8 (C and F) are available on the JCB DataViewer for observation under higher magnification.

**Online supplemental material**

Fig. S1 a shows that the nuclear structures detected with pAbN4 in U2OS cells are nucleoli, based on its colocalization with nucleolar marker fibrillarin in U2OS cells. Fig. S1 b shows that the nuclear structures detected with pAbN4 in HDFs are nucleoli, based on its colocalization with nucleolar marker fibrillarin in HDFs. Fig. S1 c shows that pAbN4 labeled nuclear rims as well as cytoplasmic foci in C2C12 myoblasts, suggesting the antibody can detect large nesprin-1 KASH nuclear envelope variants that contain SR49. Fig. S1 d shows the cytoplasmic foci in C2C12 myoblasts are

also P-bodies, based on their colocalizations with GW182. Fig. S2, a and b, show that p50$^{Nesp1}$ does not colocalize with F-actin detected by phalloidin or intermediate filaments detected by vimentin, respectively, demonstrating p50$^{Nesp1}$-bundled microtubules do not colocalize with the other major cytoskeletal filaments. Insets show enlargements. Fig. S3 shows endogenous Rck/p54 localized to PSK-1α–bundled MTs in U2OS cells expressing Myc-PSK1α. These confocal images demonstrate that the recruitment and displacement of Rck/p54 is specific to Flag-p50$^{Nesp1}$ and Flag-p50CT, respectively. Fig. S4 a shows that VSMCs express higher levels of endogenous Dcp1a, Rck/p54, and Ago2, but not GW182 or p50$^{Nesp1}$ compared with U2OS cells. GAPDH served as a loading control in these blots. Fig. S4 b shows that Rck/p54 colocalizes with Flag-p50$^{Nesp1}$ foci in si-Control VSMCs and with bundled MTs induced by RNAi of Dcp1a, suggesting expression levels of Dcp1a determine whether Flag-p50$^{Nesp1}$ localizes to P-bodies or microtubules. Fig. S4 c shows that GW182 colocalizes with Flag-p50$^{Nesp1}$ foci in si-Control VSMCs and with bundled MTs induced by RNAi of Dcp1a, suggesting GW182 localization is also determined by levels of Dcp1a. Fig. S4 d demonstrates successful knockdown of Dcp1a and low plasmid transfection efficiency of Flag-p50$^{Nesp1}$ in VSMCs. Fig. S5 shows that si-136, but not si-83, knocks down nuclear envelope nesprin-1 isoforms detected by a monoclonal antibody targeting SRs near the KASH domain of nesprin-1 in U2OS cells. These data support the lack of nuclear envelope staining observed in U2OS cells by pAbN4. Online supplemental material is available at http://www.jcb.org/cgi/content/full/jcb.201306076/DC1. Additional data are available in the JCB Data-Viewer at http://dx.doi.org/10.1083/jcb.201306076.dv.

We thank Dr. Edward Chan for his insightful comments.

We thank the Medical Research Council and British Heart Foundation for funding this work.

The authors declare no competing financial interests.

Submitted: 13 June 2013
Accepted: 17 April 2014

## References

Affaitati, A., T. de Cristofaro, A. Feliciello, and S. Varrone. 2001. Identification of alternative splicing of spinocerebellar ataxia type 2 gene. *Gene*. 267:89–93. http://dx.doi.org/10.1016/S0378-1119(01)00402-4

Aizer, A., Y. Brody, L.W. Ler, N. Sonenberg, R.H. Singer, and Y. Shav-Tal. 2008. The dynamics of mammalian P body transport, assembly, and disassembly in vivo. *Mol. Biol. Cell*. 19:4154–4166. http://dx.doi.org/10.1091/mbc.E08-05-0513

Anderson, P., and N. Kedersha. 2008. Stress granules: the Tao of RNA triage. *Trends Biochem. Sci.*33:141–150. http://dx.doi.org/10.1016/j.tibs.2007.12.003

Anderson, P., and N. Kedersha. 2009. Stress granules. *Curr. Biol.*19:R397–R398. http://dx.doi.org/10.1016/j.cub.2009.03.013

Arimoto, K., H. Fukuda, S. Imajoh-Ohmi, H. Saito, and M. Takekawa. 2008. Formation of stress granules inhibits apoptosis by suppressing stress-responsive MAPK pathways. *Nat. Cell Biol.*10:1324–1332. http://dx.doi.org/10.1038/ncb1791

Balagopal, V., and R. Parker. 2009. Polysomes, P bodies and stress granules: states and fates of eukaryotic mRNAs. *Curr. Opin. Cell Biol.*21:403–408. http://dx.doi.org/10.1016/j.ceb.2009.03.005

Bernardi, R., and P.P. Pandolfi. 2007. Structure, dynamics and functions of promyelocytic leukaemia nuclear bodies. *Nat. Rev. Mol. Cell Biol.*8:1006–1016. http://dx.doi.org/10.1038/nrm2277

Brengues, M., D. Teixeira, and R. Parker. 2005. Movement of eukaryotic mRNAs between polysomes and cytoplasmic processing bodies. *Science*. 310:486–489. http://dx.doi.org/10.1126/science.1115791

Castilla-Llorente, V., L. Spraggon, M. Okamura, S. Naseeruddin, M. Adamow, S. Qamar, and J. Liu. 2012. Mammalian GW220/TNGW1 is essential for the formation of GW/P bodies containing miRISC. *J. Cell Biol.*198:529–544. http://dx.doi.org/10.1083/jcb.201201153

Chu, C.Y., and T.M. Rana. 2006. Translation repression in human cells by microRNA-induced gene silencing requires RCK/p54. *PLoS Biol.*4:e210. http://dx.doi.org/10.1371/journal.pbio.0040210

Cottrell, J.R., E. Borok, T.L. Horvath, and E. Nedivi. 2004. CPG2: a brain- and synapse-specific protein that regulates the endocytosis of glutamate receptors. *Neuron*. 44:677–690.

Crisp, M., Q. Liu, K. Roux, J.B. Rattner, C. Shanahan, B. Burke, P.D. Stahl, and D. Hodzic. 2006. Coupling of the nucleus and cytoplasm: role of the LINC complex. *J. Cell Biol.*172:41–53. http://dx.doi.org/10.1083/jcb.200509124

Djinovic-Carugo, K., M. Gautel, J. Ylänne, and P. Young. 2002. The spectrin repeat: a structural platform for cytoskeletal protein assemblies. *FEBS Lett.*513:119–123. http://dx.doi.org/10.1016/S0014-5793(01)03304-X

Emara, M.M., K. Fujimura, D. Sciaranghella, V. Ivanova, P. Ivanov, and P. Anderson. 2012. Hydrogen peroxide induces stress granule formation independent of eIF2α phosphorylation. *Biochem. Biophys. Res. Commun.*423:763–769. http://dx.doi.org/10.1016/j.bbrc.2012.06.033

Eulalio, A., I. Behm-Ansmant, and E. Izaurralde. 2007a. P bodies: at the crossroads of post-transcriptional pathways. *Nat. Rev. Mol. Cell Biol.*8:9–22. http://dx.doi.org/10.1038/nrm2080

Eulalio, A., I. Behm-Ansmant, D. Schweizer, and E. Izaurralde. 2007b. P-body formation is a consequence, not the cause, of RNA-mediated gene silencing. *Mol. Cell. Biol.*27:3970–3981. http://dx.doi.org/10.1128/MCB.00128-07

Eystathioy, T., E.K. Chan, S.A. Tenenbaum, J.D. Keene, K. Griffith, and M.J. Fritzler. 2002. A phosphorylated cytoplasmic autoantigen, GW182, associates with a unique population of human mRNAs within novel cytoplasmic speckles. *Mol. Biol. Cell*. 13:1338–1351. http://dx.doi.org/10.1091/mbc.01-11-0544

Gros-Louis, F., N. Dupré, P. Dion, M.A. Fox, S. Laurent, S. Verreault, J.R. Sanes, J.P. Bouchard, and G.A. Rouleau. 2007. Mutations in SYNE1 lead to a newly discovered form of autosomal recessive cerebellar ataxia. *Nat. Genet.*39:80–85. http://dx.doi.org/10.1038/ng1927

Hodges, A.R., C.S. Bookwalter, E.B. Krementsova, and K.M. Trybus. 2009. A nonprocessive class V myosin drives cargo processively when a kinesin-related protein is a passenger. *Curr. Biol.*19:2121–2125. http://dx.doi.org/10.1016/j.cub.2009.10.069

Horn, H.F., Z. Brownstein, D.R. Lenz, S. Shivatzki, A.A. Dror, O. Dagan-Rosenfeld, L.M. Friedman, K.J. Roux, S. Kozlov, K.T. Jeang, et al. 2013. The LINC complex is essential for hearing. *J. Clin. Invest.*123:740–750.

Huang, J.D., S.T. Brady, B.W. Richards, D. Stenolen, J.H. Resau, N.G. Copeland, and N.A. Jenkins. 1999. Direct interaction of microtubule- and actin-based transport motors. *Nature*. 397:267–270. http://dx.doi.org/10.1038/16722

Johnston, M., M.C. Geoffroy, A. Sobala, R. Hay, and G. Hutvagner. 2010. HSP90 protein stabilizes unloaded argonaute complexes and microscopic P-bodies in human cells. *Mol. Biol. Cell*. 21:1462–1469. http://dx.doi.org/10.1091/mbc.E09-10-0885

Kedersha, N., G. Stoecklin, M. Ayodele, P. Yacono, J. Lykke-Andersen, M.J. Fritzler, D. Scheuner, R.J. Kaufman, D.E. Golan, and P. Anderson. 2005. Stress granules and processing bodies are dynamically linked sites of mRNP remodeling. *J. Cell Biol.*169:871–884. http://dx.doi.org/10.1083/jcb.200502088

Ketema, M., K. Wilhelmsen, I. Kuikman, H. Janssen, D. Hodzic, and A. Sonnenberg. 2007. Requirements for the localization of nesprin-3 at the nuclear envelope and its interaction with plectin. *J. Cell Sci.*120:3384–3394. http://dx.doi.org/10.1242/jcs.014191

Kobayashi, Y., Y. Katanosaka, Y. Iwata, M. Matsuoka, M. Shigekawa, and S. Wakabayashi. 2006. Identification and characterization of GSRP-56, a novel Golgi-localized spectrin repeat-containing protein. *Exp. Cell Res.* 312:3152–3164. http://dx.doi.org/10.1016/j.yexcr.2006.06.026

Lindsay, A.J., and M.W. McCaffrey. 2011. Myosin Va is required for P body but not stress granule formation. *J. Biol. Chem.*286:11519–11528. http://dx.doi.org/10.1074/jbc.M110.182808

Lytle, J.R., T.A. Yario, and J.A. Steitz. 2007. Target mRNAs are repressed as efficiently by microRNA-binding sites in the 5′ UTR as in the 3′ UTR. *Proc. Natl. Acad. Sci. USA*. 104:9667–9672. http://dx.doi.org/10.1073/pnas.0703820104

Marmé, A., H.P. Zimmermann, G. Moldenhauer, M. Schorpp-Kistner, C. Müller, O. Keberlein, A. Giersch, J. Kretschmer, B. Seib, E. Spiess, et al. 2008. Loss of Drop1 expression already at early tumor stages in a wide range of human carcinomas. *Int. J. Cancer*. 123:2048–2056. http://dx.doi.org/10.1002/ijc.23763

Mellad, J.A., D.T. Warren, and C.M. Shanahan. 2011. Nesprins LINC the nucleus and cytoskeleton. *Curr. Opin. Cell Biol.*23:47–54. http://dx.doi.org/10.1016/j.ceb.2010.11.006

Minshall, N., M. Kress, D. Weil, and N. Standart. 2009. Role of p54 RNA helicase activity and its C-terminal domain in translational repression, P-body localization and assembly. *Mol. Biol. Cell*. 20:2464–2472. http://dx.doi.org/10.1091/mbc.E09-01-0035

Mislow, J.M., J.M. Holaska, M.S. Kim, K.K. Lee, M. Segura-Totten, K.L. Wilson, and E.M. McNally. 2002. Nesprin-1alpha self-associates and binds directly to emerin and lamin A in vitro. *FEBS Lett.*525:135–140. http://dx.doi.org/10.1016/S0014-5793(02)03105-8

Mitsopoulos, C., C. Zihni, R. Garg, A.J. Ridley, and J.D. Morris. 2003. The prostate-derived sterile 20-like kinase (PSK) regulates microtubule organization and stability. *J. Biol. Chem.*278:18085–18091. http://dx.doi.org/10.1074/jbc.M213064200

Moser, J.J., and M.J. Fritzler. 2010. Cytoplasmic ribonucleoprotein (RNP) bodies and their relationship to GW/P bodies. *Int. J. Biochem. Cell Biol.*42:828–843. http://dx.doi.org/10.1016/j.biocel.2009.11.018

Nathans, R., C.Y. Chu, A.K. Serquina, C.C. Lu, H. Cao, and T.M. Rana. 2009. Cellular microRNA and P bodies modulate host-HIV-1 interactions. *Mol. Cell*. 34:696–709. http://dx.doi.org/10.1016/j.molcel.2009.06.003

Nonhoff, U., M. Ralser, F. Welzel, I. Piccini, D. Balzereit, M.L. Yaspo, H. Lehrach, and S. Krobitsch. 2007. Ataxin-2 interacts with the DEAD/H-box RNA helicase DDX6 and interferes with P-bodies and stress granules. *Mol. Biol. Cell*. 18:1385–1396. http://dx.doi.org/10.1091/mbc.E06-12-1120

Rajgor, D., and C.M. Shanahan. 2013. Nesprins: from the nuclear envelope and beyond. *Expert Rev. Mol. Med.*15:e5. http://dx.doi.org/10.1017/erm.2013.6

Rajgor, D., J.A. Mellad, F. Autore, Q. Zhang, and C.M. Shanahan. 2012. Multiple novel nesprin-1 and nesprin-2 variants act as versatile tissue-specific intracellular scaffolds. *PLoS ONE*. 7:e40098. http://dx.doi.org/10.1371/journal.pone.0040098

Randles, K.N., T. Lam, C.A. Sewry, M. Puckelwartz, D. Furling, M. Wehnert, E.M. McNally, and G.E. Morris. 2010. Nesprins, but not sun proteins, switch isoforms at the nuclear envelope during muscle development. *Dev. Dyn.*239:998–1009. http://dx.doi.org/10.1002/dvdy.22229

Roux, K.J., M.L. Crisp, Q. Liu, D. Kim, S. Kozlov, C.L. Stewart, and B. Burke. 2009. Nesprin 4 is an outer nuclear membrane protein that can induce kinesin-mediated cell polarization. *Proc. Natl. Acad. Sci. USA*. 106:2194–2199. http://dx.doi.org/10.1073/pnas.0808602106

Savas, J.N., A. Makusky, S. Ottosen, D. Baillat, F. Then, D. Krainc, R. Shiekhattar, S.P. Markey, and N. Tanese. 2008. Huntington's disease protein contributes to RNA-mediated gene silencing through association with Argonaute and P bodies. *Proc. Natl. Acad. Sci. USA*. 105:10820–10825. http://dx.doi.org/10.1073/pnas.0800658105

Sheth, U., and R. Parker. 2003. Decapping and decay of messenger RNA occur in cytoplasmic processing bodies. *Science*. 300:805–808. http://dx.doi.org/10.1126/science.1082320

Stewart-Hutchinson, P.J., C.M. Hale, D. Wirtz, and D. Hodzic. 2008. Structural requirements for the assembly of LINC complexes and their function in cellular mechanical stiffness. *Exp. Cell Res.*314:1892–1905. http://dx.doi.org/10.1016/j.yexcr.2008.02.022

Subramanian, R., E.M. Wilson-Kubalek, C.P. Arthur, M.J. Bick, E.A. Campbell, S.A. Darst, R.A. Milligan, and T.M. Kapoor. 2010. Insights into antiparallel microtubule crosslinking by PRC1, a conserved nonmotor microtubule binding protein. *Cell*. 142:433–443. http://dx.doi.org/10.1016/j.cell.2010.07.012

Warren, D.T., Q. Zhang, P.L. Weissberg, and C.M. Shanahan. 2005. Nesprins: intracellular scaffolds that maintain cell architecture and coordinate cell function?*Expert Rev. Mol. Med.*7:1–15. http://dx.doi.org/10.1017/S1462399405009294

Warren, D.T., T. Tajsic, J.A. Mellad, R. Searles, Q. Zhang, and C.M. Shanahan. 2010. Novel nuclear nesprin-2 variants tether active extracellular signal-regulated MAPK1 and MAPK2 at promyelocytic leukemia protein nuclear bodies and act to regulate smooth muscle cell proliferation. *J. Biol. Chem.*285:1311–1320. http://dx.doi.org/10.1074/jbc.M109.032557

Wilhelmsen, K., S.H. Litjens, I. Kuikman, N. Tshimbalanga, H. Janssen, I. van den Bout, K. Raymond, and A. Sonnenberg. 2005. Nesprin-3, a novel outer nuclear membrane protein, associates with the cytoskeletal linker protein plectin. *J. Cell Biol.*171:799–810. http://dx.doi.org/10.1083/jcb.200506083

Wu, X.S., G.L. Tsan, and J.A. HammerIII. 2005. Melanophilin and myosin Va track the microtubule plus end on EB1. *J. Cell Biol.*171:201–207. http://dx.doi.org/10.1083/jcb.200503028

Zhang, Q., J.N. Skepper, F. Yang, J.D. Davies, L. Hegyi, R.G. Roberts, P.L. Weissberg, J.A. Ellis, and C.M. Shanahan. 2001. Nesprins: a novel family of spectrin-repeat-containing proteins that localize to the nuclear membrane in multiple tissues. *J. Cell Sci.*114:4485–4498.

Zhang, Q., C. Ragnauth, M.J. Greener, C.M. Shanahan, and R.G. Roberts. 2002. The nesprins are giant actin-binding proteins, orthologous to *Drosophila melanogaster* muscle protein MSP-300. *Genomics*. 80:473–481. http://dx.doi.org/10.1006/geno.2002.6859

Zhang, Q., C.D. Ragnauth, J.N. Skepper, N.F. Worth, D.T. Warren, R.G. Roberts, P.L. Weissberg, J.A. Ellis, and C.M. Shanahan. 2005. Nesprin-2 is a multi-isomeric protein that binds lamin and emerin at the nuclear envelope and forms a subcellular network in skeletal muscle. *J. Cell Sci.*118:673–687. http://dx.doi.org/10.1242/jcs.01642